J. Fluid Mech. (1994), *vol.* 266, *pp.* 175–207

Turbulence characteristics of the boundary layer on a rotating disk

By HOWARD S. LITTELL† AND JOHN K. EATON
Department of Mechanical Engineering, Stanford University, Stanford, CA 94305, USA

(Received 15 March 1993 and in revised form 15 October 1993)

Measurements of the boundary layer on an effectively infinite rotating disk in a quiescent environment are described for Reynolds numbers up to $Re_{\delta_2} = 6000$. The mean flow properties were found to resemble a 'typical' three-dimensional crossflow, while some aspects of the turbulence measurements were significantly different from two-dimensional boundary layers that are turned. Notably, the ratio of the shear stress vector magnitude to the turbulent kinetic energy was found to be at a maximum near the wall, instead of being locally depressed as in a turned two-dimensional boundary layer. Also, the shear stress and the mean strain rate vectors were found to be more closely aligned than would be expected in a flow with this degree of crossflow. Two-point velocity correlation measurements exhibited strong asymmetries which are impossible in a two-dimensional boundary layer. Using conditional sampling, the velocity field surrounding strong Reynolds stress events was partially mapped. These data were studied in the light of the structural model of Robinson (1991), and a hypothesis describing the effect of cross-stream shear on Reynolds stress events is developed.

1. Introduction

Three-dimensional boundary layers are a common feature of engineered flow systems and their properties often limit the performance of practical devices, making the behaviour of these boundary layers of paramount importance in design. A three-dimensional boundary layer is a wall-bounded shear flow in which the mean velocity direction varies continuously with distance from the wall. In a three-dimensional boundary layer both components of velocity vary with distance from the wall, and both components of vorticity parallel to the wall are significant. Intuition suggests that a highly chaotic and three-dimensional phenomenon like boundary-layer turbulence would not be strongly affected by mean flow three-dimensionality as pointed out by Bradshaw (1970). However, a wealth of evidence shows that the turbulence structure is strongly affected by boundary-layer skewing. Conventional turbulence models fail and the present understanding of three-dimensional boundary-layer turbulence is insufficient to derive more appropriate models.

The two types of three-dimensional boundary layers of interest for this study are shown in figure 1. In figure 1 (*a*) a pressure-driven three-dimensional boundary layer is shown with the X-direction aligned with the free-stream velocity. Such a boundary layer is produced when the flow is deflected by an obstacle. The spanwise component of the pressure gradient turns the slow fluid near the wall through a greater angle than

† Present address: Shell Development Company, Houston, Texas.

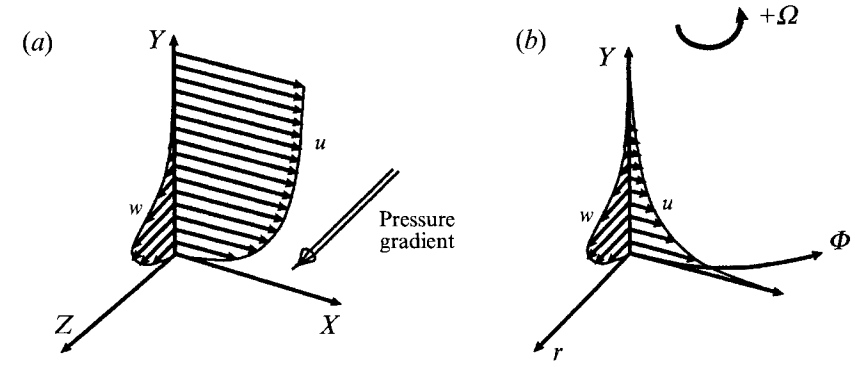

FIGURE 1. Schematic of three-dimensional velocity profiles: (*a*) pressure driven, (*b*) rotating disk.

the free stream, resulting in a skewed profile across the boundary layer. The no-slip condition is enforced at the wall so the crossflow forms a peaked velocity profile with a maximum crossflow velocity away from the wall. Figure 1(*b*) shows the three-dimensional boundary layer which forms on a rotating disk in a stationary cylindrical coordinate system. The fluid outside the boundary layer is still and the surface moves underneath it. The fluid close to the surface feels a centrifugal force in proportion to its tangential velocity, and is flung outward. The no-slip condition acts on this crossflow also, and again forces a peaked velocity profile to develop in the radial direction. This situation is analogous to the pressure-driven boundary layer described above, with the pressure gradient replaced by the centrifugal force.

The natural coordinate system of a disk flow is cylindrical, and we will use the right-handed system (r, ϕ, y). We will take advantage of the circular geometry to cancel out all derivatives of mean quantities in the ϕ-direction. However, most boundary-layer work is reported in a Cartesian coordinate system, so in order to facilitate comparison with previous experiments, the measured velocity components will be denoted

$$(U_r, U_\phi, U_y) = (-W, -U, V).$$

This choice is a result of the desire to have positive U-velocity in the rotating frame with positive rotation Ω, and is shown in figure 2.

Experiments examining three-dimensional boundary-layer turbulence are still rare. The first set of experiments to produce Reynolds stress measurements used a relaxing three-dimensional turbulent boundary layer (3DTBL) produced by a flat plate yawed at 45°, studied by Bradshaw & Terrell (1969). They discovered that even though the three-dimensionality was rather mild, the vector formed by the Reynolds stresses in the plane of the wall was not aligned with the mean flow gradient vector.† This finding invalidates the concept of a scalar-eddy viscosity. The forward-facing, 45° swept step reported by Johnston (1970), and the 'infinite' swept wing experiments of van den Berg *et al.* (1975) and Bradshaw & Pontikos (1985) showed the same behaviour. More important perhaps are changes in the Townsend structural parameter or A_1. This parameter, defined as the ratio of the shear stress vector magnitude to twice the turbulent kinetic energy, is found to have a value 0.14–0.15 for two-dimensional

† Generally in three-dimensional boundary-layer research a coordinate system is chosen with the y-coordinate normal to the wall. The two significant shear stress components $u'v'$ and $v'w'$ then form a vector in the plane of the wall as do the two strain rate components $\mathrm{d}U/\mathrm{d}y$ and $\mathrm{d}W/\mathrm{d}y$.

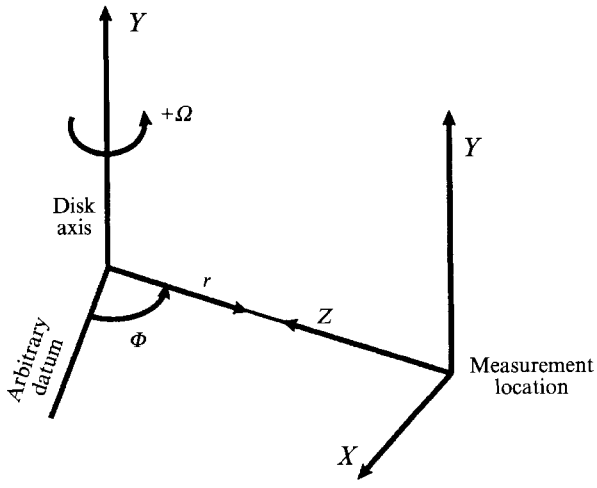

FIGURE 2. Coordinate systems used for present study.

boundary layers under quite broad circumstances. The 'infinite' swept wing experiments indicated that A_1 was considerably depressed from the two-dimensional value, especially near the wall. These two effects seem to be the common thread in 3DTBL's before they are driven to separation.

Dechow & Felsch (1977) described extensive measurements of an 'obstacle-type' flow, composed of a right cylinder on a flat plate. The shear stress angle and velocity gradient angle were seen to deviate strongly. It was found that the shear stress lags the velocity gradient until separation is approached, where the shear stress begins to clearly lead the velocity gradient. This result was supported by the experiments of Müller & Krause (1979) and Fernholz & Vagt (1981), which were also driven to separation. Anderson & Eaton (1987, 1989) described the flow of a initially two-dimensional turbulent boundary layer (2DTBL) around either a 90° or a 60° included-angle edge. The results show that A_1 decreases more rapidly with the more sudden and stronger three-dimensionality caused by the 90° wedge. The effect seen was clearly shown to be one of a drop in A_1 near the surface, with a subsequent diffusion outward of the effect. The eddy viscosity was strongly anisotropic, and comparison with other experiments led to the conclusion that experiments involving rapid skewing saw a much sharper drop in eddy viscosity ratio than those with slow turning.

In attempting to explain the Reynolds stress changes, Bradshaw & Pontikos (1985) postulated that the relative reduction of shear stress magnitude in three-dimensional boundary layers is due to the eddies being tilted out of their preferred orientation by the rate of change of $\partial W/\partial y$. It was inferred that the large eddies in a two-dimensional flow are the most efficient structures for extracting kinetic energy from the mean flow, i.e. the most efficient producers of shear stress. Shizawa & Eaton (1991), noting that the strongest changes in A_1 occurred near the wall, chose to investigate the interaction of longitudinal vortices with a three-dimensional boundary layer. It was shown that the disturbance in the velocity contours of the boundary layer is strongly dependent on the sign, or sense of rotation of the vortex. Eaton (1991) hypothesized that the same mechanism (although at a much smaller scale) may also be active in naturally formed streamwise vortices in the near-wall region. Streamwise vortices of one sign would be ineffective at producing low-speed streaks, leading to a decrease in the formation of shear stress generating events.

In addition to the physical experiments, there are now available a few direct numerical (full Navier–Stokes) simulations exploring the effect of three-dimensionality, reported by Spalart (1989), Coleman, Ferziger & Spalart (1990), Moin *et al.* (1990), Bradshaw & Sendstad (1990), and Sendstad & Moin (1991). The flow of Spalart (1989) showed no clear trend of shear stress direction compared to mean velocity gradient direction, a result that was taken to be a consequence of the near-equilibrium condition. The experiments of Coleman *et al.* showed deviations of A_1, and both leading and lagging of the shear stress direction in relation to the velocity gradient, depending on the height in the boundary layer. The last three computational studies showed that reductions in Reynolds shear stress and turbulent kinetic energy were observed as a result of a drop in production combined with an increase in dissipation. These effects were stated to be the result of the breakup of near-wall structures such as velocity streaks. Streamwise vortices are convected in the spanwise direction, breaking the original streaks. The vortices with the same sign as the developing streamwise vorticity were weakened.

It is difficult to draw general conclusions from the sum of the previous experiments because they are all complicated by extraneous effects such as streamwise pressure gradient and spanwise inhomogeneity. It is generally agreed that the misalignment of the shear stress and strain rate vectors is an effect of rapid turning of the flow. However, there is disagreement on the cause of the relative reduction in magnitude of the shear stress. Some investigators believe that this is also an effect of the rapid turning while others think that it is a general effect of a three-dimensional strain field. Experiments and simulations examining the structure of the turbulence are at such an early stage that there is at present no consensus regarding structural modifications.

The flow over a rotating disk was chosen for the present study, to address some of the concerns expressed about previous experiments. The analysis of the turbulence data is considerably simplified using the disk geometry. The disk rotates in a quiescent environment so there are no externally imposed pressure gradients, and the flow is axisymmetric so only two space coordinates are needed to describe the mean flow. Also, variation in the radial direction is very small, and can usually be neglected except near transition. The mean flow develops substantial skewing across the boundary layer; at its peak the crossflow reaches 11% of the local disk speed, so the three-dimensionality must be considered a major feature of the flow.

There are key differences between previously studied 3DTBL's and the disk boundary layer. First, the three-dimensionality is present continuously; it does not develop from an initially two-dimensional boundary layer. This is important for investigating structural differences between 3DTBL's and 2DTBL's, since the modification of two-dimensional structures is not an issue. Secondly, the turbulence may reach an equilibrium with the imposed three-dimensional strain field. Finally, the rotation which drives the flow adds Coriolis effects to the basic equation set, both complicating analysis and possibly modifying the turbulence itself.

The laminar flow field above an infinite rotating disk was first considered by von Kármán (1921), who deduced that the flow could be described by a similarity solution. Experimental velocity profiles measured on finite disks agree well with the predictions. The laminar flow field has a crossflow (radial) profile with an inflexion point, which is unstable and eventually breaks down into turbulent flow (cf. Kohama 1987; Wilkinson & Malik 1985; and Kobayashi, Kohama & Takamadate 1980).

Early work on turbulent disk flows was performed by Goldstein (1935), Theodorsen & Regier (1944), Gregory, Stuart & Walker (1955), Cobb & Saunders (1956), and Case (1966). The most comprehensive study to date for an 'infinite' disk flow was published

by Cham & Head (1969). They reported single hot wire and Pitot probe surveys for $Re = 2000000$, with local Reynolds number defined as

$$Re = \Omega r^2/\nu.$$

Integral boundary-layer calculations and an isotropic eddy viscosity calculation of the crossflow profiles both showed good agreement with the experimental data. Erian & Tong (1971) acquired mean velocities, turbulent intensities, and one Reynolds shear stress for a turbulent disk flow. They employed a questionable hot-wire technique which included aligning a single wire with the circumferential direction in order to measure cross-stream velocity fluctuations, almost certainly yielding erroneous readings. Cebeci & Abbott (1975) published results of a calculation of the disk flow using isotropic eddy viscosity, which compared well with those of Cham & Head for mean velocity and skin friction, but did not match well with those of Erian & Tong for the crossflow near the wall.

In an experiment related to the flow over an infinite rotating disk, Itoh *et al.* (1990) studied an enclosed disk with a shroud at the periphery and a stationary facing disk at a small separation $s/R = 0.08$. The direction of the shear stress vector was found not to coincide with the mean velocity gradient vector, in agreement with previous three-dimensional boundary layer experiments. The Townsend structure parameter was near 0.15 near the disk, but fell slowly as height increased.

Summarizing the existing state of knowledge of three-dimensional boundary layers we find that high-quality experiments have been performed on a number of different geometries. Generally observed trends are that the shear stress is suppressed relative to the turbulent kinetic energy and that when the free stream turns monotonically, the shear stress vector lags behind the strain rate. The reasons for these trends have not been satisfactorily explained and inferences about the turbulence structure have been based entirely on single-point statistical measurements. For the three-dimensional boundary layer on a rotating disk the mean flow behaviour is well understood but even the single-point turbulence measurements are incomplete.

The objectives of the study are to document the turbulence structure over an 'infinite' rotating disk through the acquisition of detailed mean velocity data and turbulence measurements up to third-order quantities. An important question is: Are the commonly observed effects of three-dimensionality still present when a boundary layer develops as three-dimensional from its inception? The disk flow should be large enough that the turbulence is in equilibrium with the three-dimensional strain field unlike previous experiments in which the three-dimensional boundary layer developed by distorting a two-dimensional boundary layer. In addition, the turbulence structure was studied using multipoint measurements. The objective was to gain some insight into the differences in the turbulence structure between two- and three-dimensional boundary layers. In this case we take as the baseline the extensive body of work on two-dimensional boundary-layer structure. This work is not reviewed here; the reader is referred to the recent review of Robinson (1991).

2. Facility and experimental techniques

The experiments were performed on a 1 m diameter disk rotating on a vertical axis in a nominally quiescent environment. A cast aluminium tooling plate disk was machined to a finished thickness of 15 mm and lapped to a surface finish of 10 μm. The disk was mounted on a vertical spindle that was driven at speeds up to 1500 r.p.m. The vertical runout was measured at a radius of 0.48 m using a dial indicator. The runout

of ± 15 μm was in the form of long-wavelength variation on the disk and a slight cyclic rise and fall with a period of several rotations due to imperfections in the roller bearings. The horizontal runout was measured to be less than ± 25 μm.

The disk apparatus was mounted in a $2.4 \times 2.7 \times 3.4$ m isolation cell. A fixed annular apron approximately 0.3 m wide surrounded the disk to eliminate any interaction between the boundary layers on the top and bottom surfaces. The bottom surface ran in a closed cavity to avoid creating any disturbance in the test cell. A set of 14 spiral-shaped vanes were mounted on the upper surface of the apron to remove the angular momentum of the flow leaving the disk. No significant swirl was observed in the test cell with the vanes in place.

The computer-controlled probe traverse was mounted on a 1×4 in. steel beam located 1 m above the disk surface and isolated from the disk carriage to eliminate vibrations. The probe traverse could rotate the probe about a vertical axis in 0.9° increments and traverse the probe normal to the disk with a resolution of 1.6 μm. All experiments were conducted remotely to minimize disturbance of the flow.

The mean flow velocity and direction were measured using three redundant techniques: a three-hole probe, a single hot-wire probe and a custom dual-wire probe. The three-hole probe was used in a non-nulling mode as described by Anderson & Eaton (1987). The dynamic and differential pressures were measured using Setra model 239 (± 1.0 in. H_2O range) or a model 264 (0–10 in. H_2O range) pressure transducers calibrated against a micromanometer before each run. Corrections for both the effect of mean shear on the effective probe location and the effect of wall proximity on angle measurements were applied. Both these corrections were calibrated by matching the data to the analytical solution for the laminar boundary layer. The angular uncertainty of the three-hole probe was quoted by Anderson & Eaton (1987) as $\pm 1.0°$. The uncertainty in velocity was given as ± 0.2 m s^{-1} which would decrease in magnitude for the very low velocities at the edge of the boundary layer, although the percentage uncertainty would certainly increase.

The single-wire probe used a Dantec 55P05 boundary-layer tip strung with Dantec gold plated 5 μm platinum-coated tungsten wire with an active length to diameter ratio of $l/d = 250$. This probe was used to determine the velocity and the angle of the flow by yawing it to several different angles in a procedure similar to that of Cham & Head (1969). The procedure was performed automatically under computer control and resulted in an uncertainty of $\pm 1.5°$. A second probe with two wires in the same plane parallel to the wall was built to provide redundant measurements. Construction details and the calibration procedure are described in Littell & Eaton (1991*b*). The uncertainty was found to be the same as for the single wire and the measurements from the two probes agreed to well within the uncertainty estimate at every measurement position.

Turbulence data were measured using a miniature single-wire probe and a set of cross-wire probes. The single-wire probe used 2.5 μm platinum-coated tungsten wire which was copper plated and subsequently etched for an active length to diameter ratio of $l/d = 220$. The probe size was selected following the recommendations of Ligrani & Bradshaw (1987). The measurement volume of dimension $l^+ = 35$ at $Re = 650000$ should give relatively small errors in turbulence statistics at the y^+ distances reported here. The crosswire probes were custom built to use the 2.5 μm wire with a wire spacing of 0.35 mm, following dimensional guidelines shown in the literature to yield the most accurate results. These design parameters were used to build the most compact crosswire probe possible which would have truly negligible blockage and interference, a necessity for the highly turbulent flow on the disk. The crosswires could be rotated about their axes in 45° increments allowing determination of all six Reynolds stresses.

Quantity	Uncertainty (aligned)	Error from 5° misalignment
$\overline{U}$	3% of $\overline{U}$	1% of $\overline{U}$
$\overline{u'^2}$	5% of $\overline{u'^2}$	4% of $\overline{u'^2}$
$\overline{v'^2}$	5% of $\overline{u'^2}$	4% of $\overline{u'^2}$
$\overline{w'^2}$	5% of $\overline{u'^2}$	4% of $\overline{u'^2}$
$\overline{u'v'}$	10% of $\overline{u'v'}$	7.5% of $\overline{u'v'}$
$\overline{v'w'}$	15% of $\overline{u'v'}$	8.5% of $\overline{u'v'}$
$\overline{u'w'}$	10% of $\overline{u'v'}$	7.5% of $\overline{u'v'}$

TABLE 1. Crosswire uncertainties from Anderson & Eaton (1987)

The hot wires used were all run in constant-temperature mode by a TSI IFA-100 unit, or in the case of the two-point correlations, one crosswire was run by a pair of Dantec 55M01 units. After DC shifting and amplification, the signals were low-pass filtered with a Frequency Devices model 901F1, usually with a corner frequency of 29.9 kHz. A temperature-dependent calibration was obtained by varying both the temperature and velocity and fitting King's law in a modification of the temperature correction suggested by Cimbala & Park (1990); a complete discussion is given in Littell & Eaton (1991*b*). The effective wire angles were found by assuming cosine response and yawing the probe in the calibration jet as described in Westphal & Mehta (1984). The total uncertainty of the mean velocities measured by the hot-wire methods was estimated to be $< 2\%$ near the disk, and would be expected to rise significantly in the intermittent region of the outer boundary layer owing to free convection effects from the hot wire which would be indistinguishable from a velocity measurement.

The uncertainties in the measured turbulence quantities are the same as quoted by Anderson & Eaton (1987) near the wall where the turbulence intensity is similar to flat-plate boundary-layer values. These are summarized in table 1. These uncertainties are expected to rise rather quickly with distance from the wall, and to have perhaps doubled in most categories by a turbulence intensity of 40%, which translates as $y/\delta_2 \approx 5$. The increased uncertainty was estimated based on a simulated crosswire response following the general methodology of Tutu & Chevray (1975) (see Littell & Eaton 1991*b*). Comparison of their assumptions to the actual measured quantities suggests that the Tutu & Chevray analysis is somewhat pessimistic in the present situation.

The data acquisition and control system consisted of an IBM PC-AT and a Metrabyte DAS-20 12 bit A/D card equipped with a SSH-4 simultaneous sample and hold. The computer was used to control the speed of the disk and the motion of the traverse, and to acquire, analyse, and store the various measurements of interest.

3. Mean velocity

Mean velocity data taken with a hot wire are shown in figures 3(*a*) and 3(*b*) for several Reynolds numbers. Three-hole probe data agreed closely so are not shown here. Figure 4 shows a 'polar' plot of the crossflow velocity versus the streamwise velocity as measured by the hot-wire techniques. The plot suggests a weak effect of Reynolds number on the crossflow profile at a given radius. Similar, but much stronger, trends were observed in the rapidly skewing flow studied by Anderson & Eaton (1987, 1989). In that flow the crossflow increases owing to the sustained pressure gradient but the location of the peak also moves towards the higher streamwise

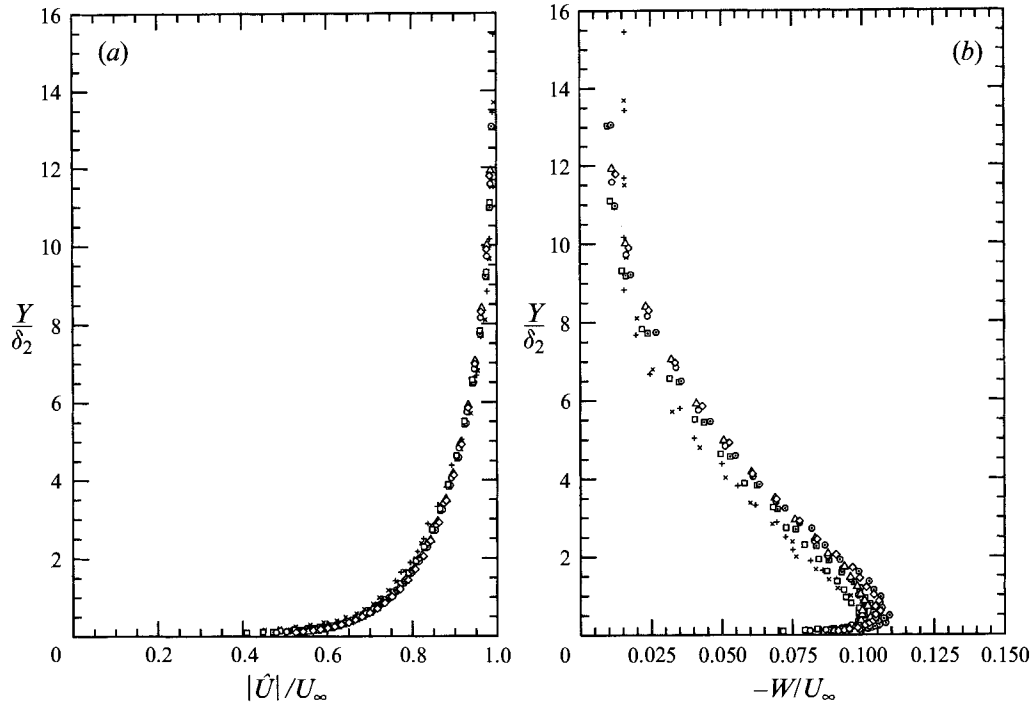

FIGURE 3. (*a*) Turbulent mean flow vector magnitude in the rotating reference frame as measured by the hot-wire probes. (*b*) Crossflow profile measured by the hot wires in turbulent regime. Symbols on this and subsequent figures are defined in table 2.

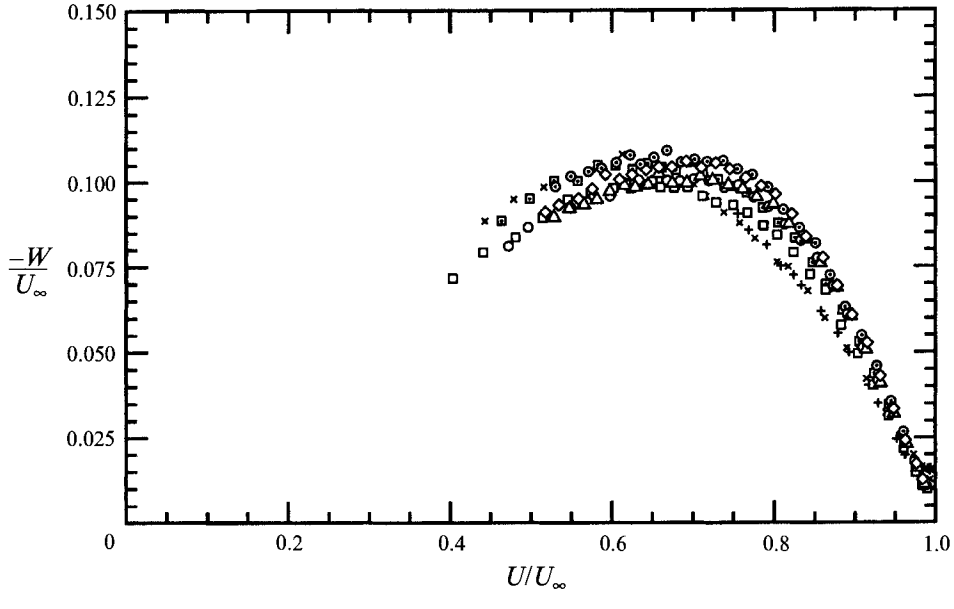

FIGURE 4. Polar plot of turbulent velocity profiles measured by hot-wire probes.

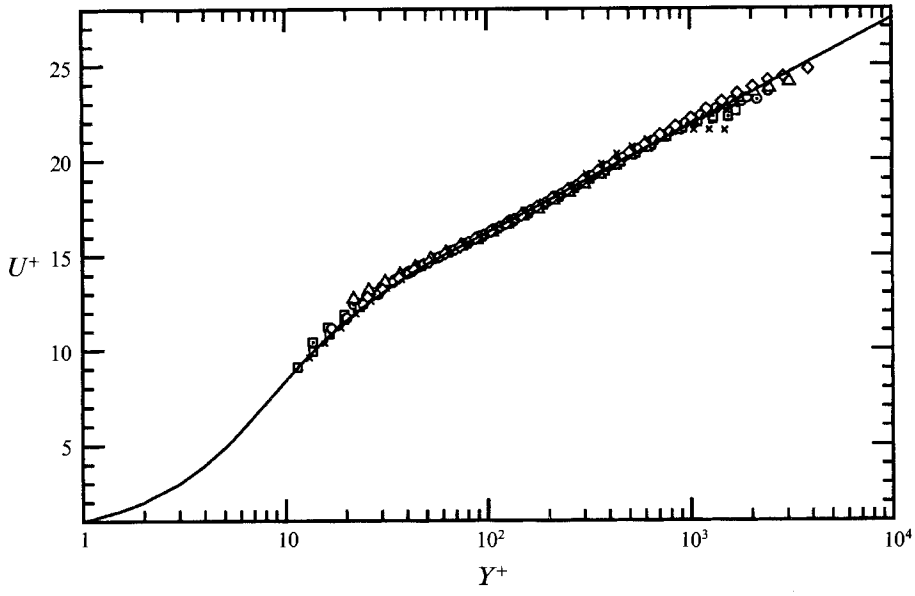

FIGURE 5. Tangential velocity plotted in wall coordinates for the rotating coordinate system.

velocity. Driver & Johnston's (1990) experiment in which a shear-driven 3DTBL is relaxing back to a two-dimensional layer shows the same effect. The Squire–Winter (1951) theorem relates the crossflow profile in the outer part of the boundary layer to free-stream skewing angle from purely kinematic considerations. This relationship is

$$W/U_\infty = 2\alpha(1-U/U_\infty), \tag{1}$$

where α is the angle through which the original free stream has been turned. This equation describes the amount of crossflow developed by inviscid skewing of the pre-existing spanwise vorticity. The peak crossflow velocity would occur at the wall by (1) but is limited by the no-slip condition and thus occurs above the wall. The crossflow momentum deficit is continuously diffusing outward, so if the skewing stops then the peak must progress outward too. The shear-driven flow of Driver & Johnston (1990) exhibits this behaviour. The disk flow differs in that its three-dimensionality is being forced continuously, but not with an increasing skewing angle. This gives us a chance to look at the motion of the peak crossflow in a three-dimensional flow that is close to equilibrium. The peak is not scaling on inner variables, since its height increases, or at least stays the same, in figure 3(*b*) as the Reynolds number increases. The establishment of outer scaling is not indicated, since the total thickness of the boundary layer is difficult to measure experimentally owing to the very low velocities at the edge of the boundary layer.

The tangential mean velocity profile is plotted in semi-log coordinates in figure 5 with the conventional two-dimensional law of the wall:

$$U^+ = 2.44 \ln y^+ + 5.0. \tag{2}$$

Also shown is the Van Driest model for the buffer region. The vector magnitude of the velocity was also plotted in wall coordinates, and is virtually indistinguishable from figure 5. The only real difference between these data and those of a high-Reynolds-number 2DTBL is the lack of a wake component. In a 2DTBL the absence of a wake

Symbol	R (m)	Re	U_∞ (m s^{-1})	δ_{99} (mm)	δ_2 (mm)
+ ×	0.235	400000	26.1	11.6	0.98
⊡	0.356	650000	28.2	19.2	1.46
⊙		940000	41.0	20.0	1.46
□	0.421	650000	23.7	21.0	1.71
○		1000000	36.7	20.6	1.64
△		1300000	48.1	20.4	1.59
◇		1600000	59.1	21.4	1.61

Symbol	Re_{δ_2}	H	G	$U\tau$ (m s^{-1})	ν/U_τ (μm)
+ ×	1660	1.34	5.52	1.21	12.8
⊡	2660	1.29	5.06	1.26	12.3
⊙	3840	1.27	4.97	1.75	8.9
□	2640	1.30	5.18	1.05	14.6
○	3900	1.28	5.19	1.56	9.9
△	4970	1.27	5.12	2.00	7.7
◇	6070	1.27	5.22	2.39	6.6

TABLE 2. Disk flow turbulent cases

would signal the presence of a streamwise favourable pressure gradient. The disk cannot support a pressure gradient in the tangential direction, so the cause of the lack of a wake is unclear. Streamwise profiles of Cham & Head (1969) were plotted in wall coordinates, and likewise do not exhibit a conventional wake, but seem to have either a very short log region or a different slope than the two-dimensional law of the wall. Senoo & Nishi (1972) described a pressure-driven endwall flow which was turned through a large angle to investigate the properties of an equilibrium 3DTBL. Their data showed absolutely no wake component in the equilibrium region, and they concluded that this indicated a lack of reliance on the upstream flow properties. In the disk flow, the vertical component of velocity, V, is negative with an estimated value of 0.6% of U based on the entrainment measurements of Cham & Head (1969). This downflow would tend to increase the strength of the wake by bringing outer-layer fluid towards the wall, but clearly the logarithmic region dominates and suppresses the formation of a wake.

Several common integral parameters and descriptors of the mean tangential flow are given in table 2. These were calculated using an analytic integration of a natural cubic spline fit to the experimental data, with the Van Driest model inserted below $y^+ = 50$ in order to extend the measurements to the wall. Owing to the relatively small crossflow, the same data for the vector magnitude profile are not significantly different. A constant value of the Clauser shape factor G means that the outer region of the boundary layer is self-similar and, by the data in table 2, it appears the disk boundary layer is such an 'equilibrium' flow with $G \approx 5.2$. A flat-plate boundary layer exhibits $G = 6.6$–6.8; a higher value indicates adverse pressure gradient, and a lower value indicates favourable pressure gradient.

4. Turbulence characteristics

The Reynolds stresses were acquired using the crosswise probe aligned with the previously measured mean flow angle at each measurement position and subsequently transformed into the disk frame of reference. Figure 6 shows all three normal stresses

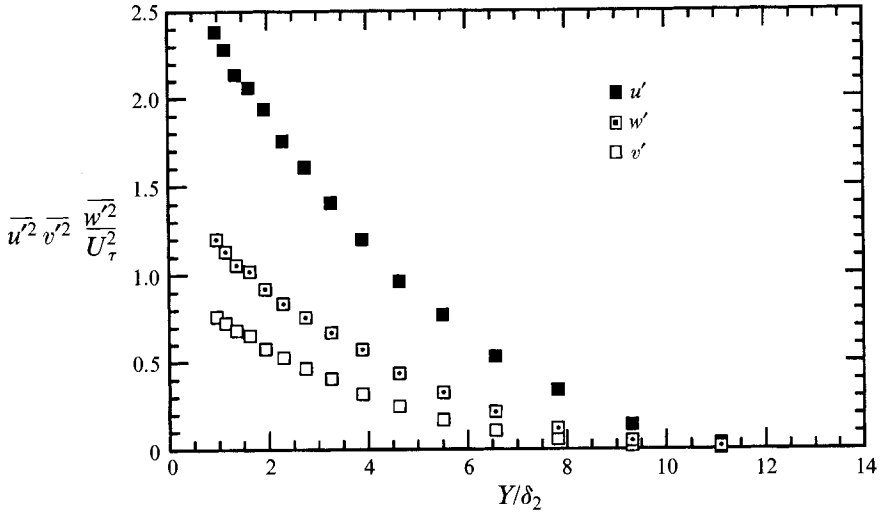

FIGURE 6. Normal Reynolds stresses *vs.* Y/δ_2 at $Re = 650000$.

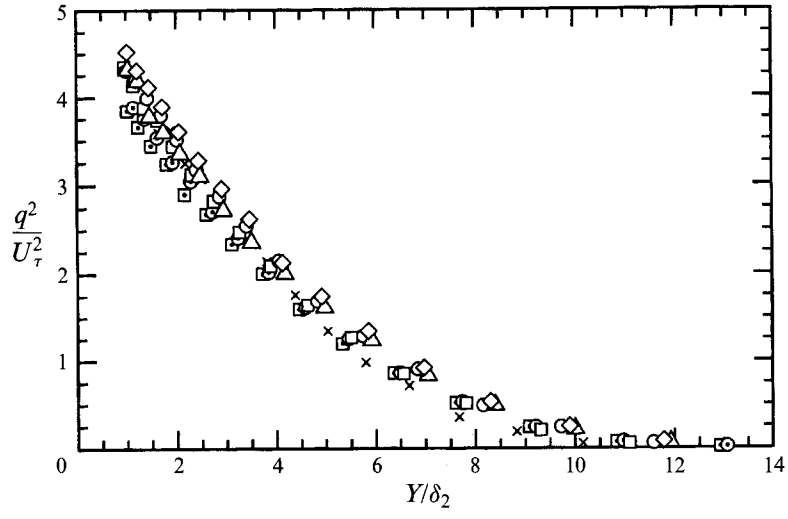

FIGURE 7. Twice the turbulence kinetic energy q^2 *vs.* Y/δ_2.

at a single Reynolds number to indicate the relative magnitude of the components. The abscissa is scaled by δ_2 instead of δ_{99} because the latter is very difficult to measure in this flow. The tangential friction velocity u_τ obtained from the log-law fit is used to scale the ordinate. Streamwise turbulent fluctuations measured by the crosswire were somewhat lower than those measured by a single hot wire, but agreed to within the accuracy given in table 1. The single-wire data cannot be transformed into the disk coordinate frame so they are not shown in figure 6.

The trace of the Reynolds stress tensor, q^2, equal to twice the turbulent kinetic energy is shown in figure 7. In many 3DTBL studies which involve turning an initially two-dimensional boundary layer the turbulent kinetic energy is seen to decrease with increasing three-dimensionality. In this flow the three-dimensionality is applied constantly, which may explain why the normalized value of q^2 is constant with

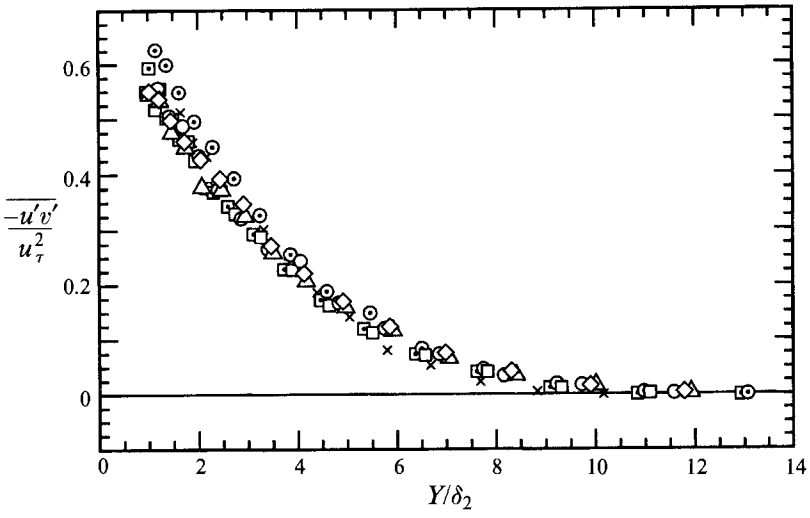

FIGURE 8. $\overline{u'v'}/u_\tau^2$ (or $-\overline{u'_\phi u'_y}/u_\tau^2$) Reynolds shear stress *vs.* Y/δ_2.

increasing Reynolds number. A small shift with Reynolds number is not ruled out, at least with the scaling employed, but since the momentum-thickness Reynolds number more than triples it is probably a safe conclusion that the turbulent kinetic energy in the outer region of the disk boundary layer is not changing significantly with Reynolds number.

The primary Reynolds shear stress $-\overline{u'v'}$ is shown in figure 8. For two-dimensional boundary layers this shear stress generally extrapolates to the wall shear stress; this has a value of 1.0 on this ordinate. It is often assumed that the shear stress is constant across the log region for zero-pressure-gradient boundary layers. In fact, the shear stress actually decreases slowly; Klebanoff (1954) measured a shear stress value of $0.85u_\tau^2$ at $y/\delta = 0.2$. In the present study the shear stress decreases much more rapidly: $-\overline{u'v'}$ is less than $0.5u_\tau^2$ at $y/\delta = 0.2$ ($y/\delta_2 \approx 2$). Even smaller shear stress values were found by Itoh *et al.* (1990) in a study of a shrouded disk. The present results also differ considerably from previous studies of pressure-driven 3DTBL's. Most of these flows exhibit a peak in the shear stress well away from the wall. This effect cannot be ascribed only to an adverse pressure gradient, but is also a sign of a structural change in the turbulence. The primary shear stress in this flow is seen to be unlike either a 2DTBL or other 3DTBL's, suggesting major differences in the structure to be discussed more fully below.

The secondary shear stress $-\overline{v'w'}$, also normalized by the friction velocity, is shown in figure 9. This quantity is identically zero in a 2DTBL. The present measurements show $\overline{v'w'}$ to be almost constant in the region where the crosswire could acquire data, but it must change sign closer to the wall in order to approach the spanwise wall shear stress. These measurements resemble previous 3DTBL experiments plotted in free-stream coordinates. The data of Itoh *et al.* (1990) show basically the same nearly constant $-\overline{v'w'}$ stress layer as seen here.

The third shear stress component, $\overline{u'w'}$ is also non-zero in 3DTBL's. This stress gradient is generally neglected in the boundary-layer approximations for the velocity components parallel to the wall since it is usually much smaller than gradients of the other two shear stresses. The derivative of this term with respect to radius was evaluated and found to be more than two orders of magnitude smaller than the

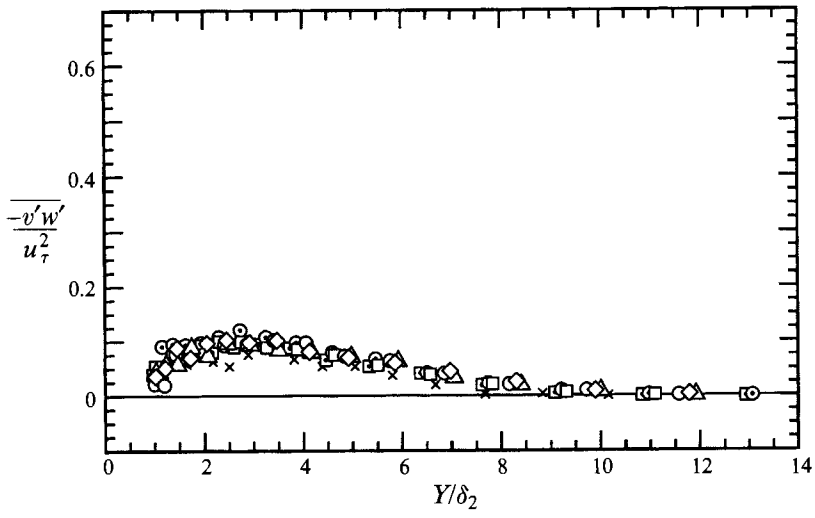

FIGURE 9. $\overline{v'w'}/u_\tau^2$ (or $-\overline{u'_\phi u'_r}/u_\tau^2$) Reynolds shear stress *vs.* Y/δ_2.

Symbol	Experiment	Flow type/designation
A	Anderson & Eaton (1989)	Obstacle, Case I St 4
D	Dechow & Felsch (1977)	Obstacle, St 4
P	Bradshaw & Pontikos (1985)	Infinite wing, $X = 1092$
R	Driver & Johnston (1990)	Shear driven, St 9
E	Elsenaar & Boelsma (1974)	Infinite wing, $X = 1095$

TABLE 3. Reference experiments

derivative of $\overline{u'v'}$ with respect to the wall normal, in the near-wall region, and at least a factor of 20 smaller at $Y/\delta_2 = 7$. For this reason it does not play a significant role in the mean velocity profile development, and will not be shown here.

Previous experiments on 3DTBL's have shown that dimensionless structural parameters used in closure models for the Reynolds stresses may be strongly modified from typical 2DTBL values. The present measurements are compared to other types of 3DTBL's in the following paragraphs. The data sets selected for comparison are listed in table 3. This set includes each of the three major categories of 3DTBLs: infinite swept wing, obstacle, and shear driven. The choice of coordinate system is often important in such comparisons. It is natural to select one coordinate direction normal to the wall, but the orientation of the other axes is relatively arbitrary in 3DTBL's. For this reason, the structural parameters which prove most useful are those that are invariant to rotation about the wall normal.

A commonly investigated structural parameter is the ratio of the vector magnitude of the shear stress to twice the turbulent kinetic energy:

$$A_1 = \frac{(\overline{u'v'}^2 + \overline{v'w'}^2)^{\frac{1}{2}}}{q^2}.$$

This parameter is approximately constant at 0.15 in a 2DTBL even when the layer is distorted by a pressure gradient, except very near the wall under an adverse pressure gradient. The wind tunnel experiments plotted in figure 10 show the typically observed

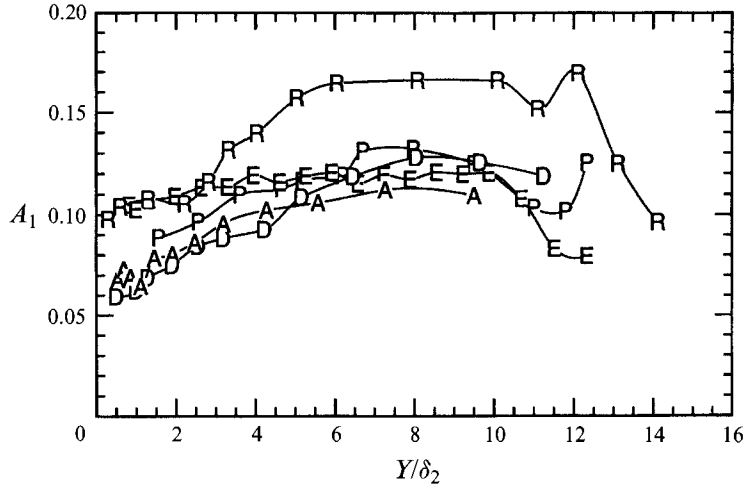

FIGURE 10. Structural parameter A_1 *vs.* Y/δ_2 for reference 3DTBL studies listed in table 3.

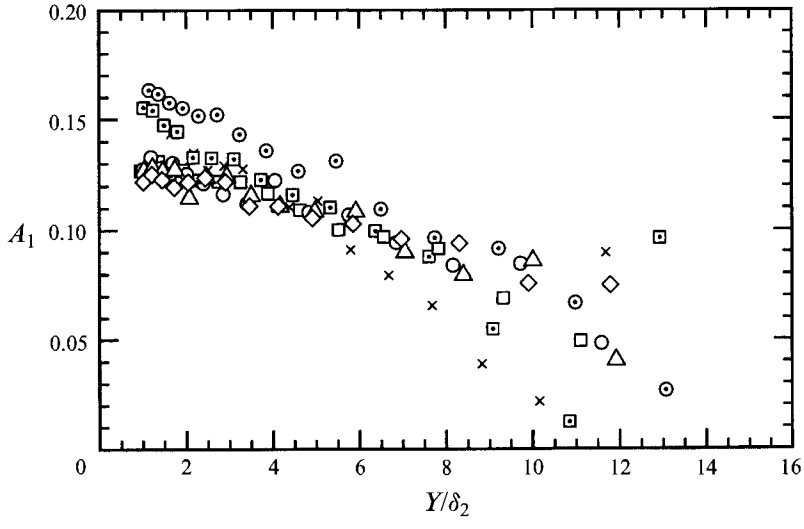

FIGURE 11. Structural parameter A_1 *vs.* Y/δ_2 for present study.

trend that three-dimensionality depresses A_1 near the wall, and this depression diffuses outward. Figure 11 indicates a different behaviour in the disk flow, showing A_1 to decrease almost linearly with distance from the wall for the inner radii, and at least monotonically for the outer radius. Similar results were found in the direct numerical simulation of an Ekman layer by Coleman *et al.* (1990). Examining the flow at the pole of a sphere they found a peak value of A_1 equal to 0.12 close to the surface, falling with a constant slope to 0.065 at the edge of the Ekman layer. The strong attenuation of A_1 suggests that irrotational (inviscid) motions dominate the outer region of the disk boundary layer. It must be pointed out that the present outer-region measurements may be subject to large errors according to Tutu & Chevray (1975), which could account for part of the effect seem on A_1.

One might suspect that the outer region of the boundary layer is dominated by Coriolis effects. The Reynolds stress transport equations for a rotating coordinate

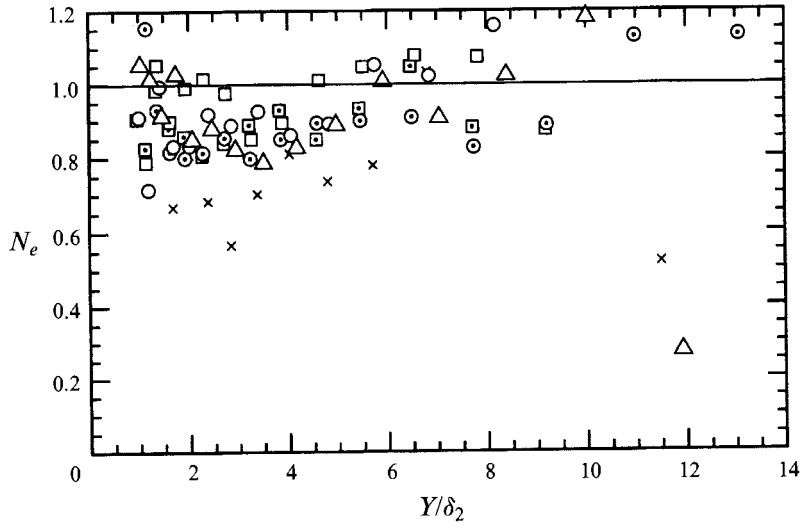

FIGURE 12. Eddy viscosity ratio N_e.

system show that Coriolis effects act to redistribute the Reynolds stress among the various components of the tensor. If the outer region were dominated by Coriolis effects, then w' and u' fluctuations must be negatively correlated. However, the correlation coefficient for $\overline{u'w'}$ was calculated and is strongly positive in the outer layer, indicating that Coriolis effects are not a major factor. This then supports the conclusion that the outer region is dominated by irrotational (inviscid) motions, a conclusion also supported by Cham & Head's (1969) measurement of reduced entrainment.

It is often found in three-dimensional boundary-layer experiments that the eddy viscosity is not isotropic, that is

$$\frac{-\overline{v'w'}}{\partial W/\partial y} \neq \frac{-\overline{u'w'}}{\partial U/\partial y}.$$

As a measure of this inequality, the ratio of the eddy viscosities can be written as

$$N_e = \frac{\tan(\gamma_\tau - \gamma_{fs})}{\tan(\gamma_g - \gamma_{fs})},$$

where γ_{fs} is the angle of the local mean velocity, γ_g is the angle of the velocity gradient vector, and γ_τ is the shear stress vector angle. Clearly, the choice of coordinate system is important here. In this case we have referenced all angles to the free stream velocity direction. The values obtained for N_e are shown in figure 12. These data exhibit more scatter than most of the other plots because they contain derivatives of experimental data. As concluded by Anderson & Eaton (1989), low values of N_e (as low as 0.2) are observed in sharply turned experiments such as shear-driven or obstacle flows, and a value closer to unity is seen in slowly turned flows like the infinite wing. This implies that the disk flow more closely resembles a slowly turned flow or equivalently one that has more time to relax to a new state after the imposition of crossflow. The values near unity indicate that an isotropic eddy viscosity should perform well, and this was indeed the case for a simple crossflow calculation for the disk flow reported by Cham & Head (1969), and a more involved calculation by Cebeci & Abbott (1975).

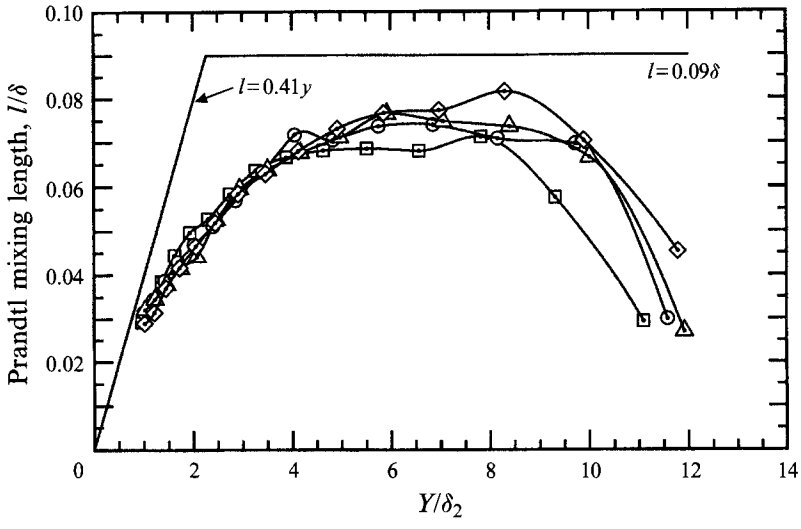

FIGURE 13. Prandtl mixing length *vs.* typical two-dimensional behaviour; $r = 0.421$.

A mixing length for three-dimensional boundary-layer turbulence may be defined as

$$(\overline{u'v'}^2+\overline{v'w'}^2)^{\frac{1}{2}} = l^2\left[\left(\frac{\partial U}{\partial y}\right)^2+\left(\frac{\partial W}{\partial y}\right)^2\right]. \tag{3}$$

This mixing length is thus invariant to rotation of the coordinates about the wall normal direction. Figure 13 shows the mixing-length distribution across the disk boundary layer plotted along with the commonly used correlations for 2DTBL's. The mixing length falls well below the standard log-region correlation, $l = 0.41y$, again illustrating the suppression of shear stresses in this flow and the absence of a constant stress layer. The pressure-driven experiments from table 3 deviate from the 2DTBL correlations in the same way as the present data and in particular asymptote to mixing lengths well below $l/\delta = 0.09$. Suppressed mixing length and a thinned constant-stress layer thus appear to be common features of pressure-driven 3DTBL's.

Dissipation lengthscales were calculated from the data and the models of Bradshaw, Ferris & Atwell (1967) and Hunt, Spalart & Mansour (1987). Detailed comparisons are presented in Littell & Eaton (1991*b*). These corroborate the conclusion that lengthscales are reduced by three-dimensionality and indicate that the turbulent kinetic energy budget is similar to that of a 2DTBL, while the shear stress is modified by three-dimensionality.

Some insight into the differences between 2DTBL's and 3DTBL's may be obtained by examining the terms in the Reynolds stress transport equations. It is appropriate to examine the present data using cylindrical rotating coordinates but we have chosen here to write the equations with the more familiar Cartesian velocities and axes to facilitate comparison with other flows. Some of the terms in these equations resulting from the cylindrical coordinate system are negligible for this large radius, but are included here to retain the generality of the equation set. The derivatives of mean quantities with respect to the tangential direction are identically zero, and certain terms are neglected by order of magnitude arguments in the usual fashion. In the equations below, the terms are grouped into sets in the usual way as described in Littell & Eaton (1991*b*).

For $\overline{u'v'}(=-\overline{u'_\phi u'_y})$:

$$\frac{\partial(-\overline{u'v'})}{\partial t} = 0 = \left(V\frac{\partial}{\partial y} + W\frac{\partial}{\partial z}\right)\overline{u'v'} - U\frac{\overline{v'w'}}{r} \quad \text{advection}$$

$$+2\Omega\overline{v'w'} \quad \text{rotation}$$

$$+\overline{v'^2}\frac{\partial U}{\partial y} - W\frac{\overline{u'v'}}{r} + \overline{v'w'}\frac{\partial U}{\partial z} \quad \text{production}$$

$$-2\frac{\overline{u'v'w'}}{r} + \frac{\partial\overline{u'v'v'}}{\partial y} \quad \text{diffusion}$$

$$+D; \quad \text{dissipation}$$

for $\overline{v'w'}(=-\overline{u'_y u'_r})$:

$$\frac{\partial(-\overline{v'w'})}{\partial t} = 0 = \left(V\frac{\partial}{\partial y} + W\frac{\partial}{\partial z}\right)\overline{v'w'} + U\frac{\overline{u'v'}}{r} \quad \text{advection}$$

$$-2\Omega\overline{u'v'} \quad \text{rotation}$$

$$+\overline{v'^2}\frac{\partial W}{\partial y} + U\frac{\overline{u'v'}}{r} + \overline{v'w'}\frac{\partial W}{\partial z} \quad \text{production}$$

$$+\frac{\overline{u'u'v'}}{r} - \frac{\overline{v'w'w'}}{r} + \frac{\partial\overline{v'v'w'}}{\partial y} \quad \text{diffusion}$$

$$+D; \quad \text{dissipation}$$

for q^2:

$$\frac{\partial q^2}{\partial t} = 0 = \left(V\frac{\partial}{\partial y} + W\frac{\partial}{\partial z}\right)q^2 \quad \text{advection}$$

$$-2\left(+\frac{W}{r}\overline{u'u'} - \frac{U}{r}\overline{u'w'} - \overline{v'w'}\frac{\partial W}{\partial y} - \overline{u'v'}\frac{\partial U}{\partial y}\right) \quad \text{production}$$

$$+\frac{\partial}{\partial y}(\overline{u'u'v'} + \overline{v'v'v'} + \overline{v'w'w'}) \quad \text{diffusion}$$

$$+D. \quad \text{dissipation}$$

The dissipation group is evaluated here as the difference of the other terms. In making this approximation is must be recognized that the pressure diffusion and the pressure strain terms (0 in the q^2 equation) that are not dissipative are included, since these are likewise not measured. The viscous diffusion term is simply neglected.

The terms involving derivatives of the data were computed by smoothing the experimental results as described in Littell & Eaton (1991*a*), while the measured quantities that appear in the equations were not smoothed. Terms involving derivatives in the radial direction were calculated to be two orders of magnitude less than the typically retained terms, and were neglected.

The transport balance of the primary shear stress for a Reynolds number of 1 300 000 is shown in figure 14(*a*). The values are normalized by δ/u_τ^3 where $\delta = \delta_2/0.097$. The data are plotted with a gain in $-\overline{u'v'}$ positive, and a loss negative. If these are compared with typical 2DTBL shear stress balances, such as the direct Navier–Stokes calculation of Spalart (1988), it is apparent that the production of $-\overline{u'v'}$ is concentrated much nearer the surface, indicating that the outer region is dominated by inactive motion. A clear structural feature noted in the numerical data is an increase in turbulent diffusion

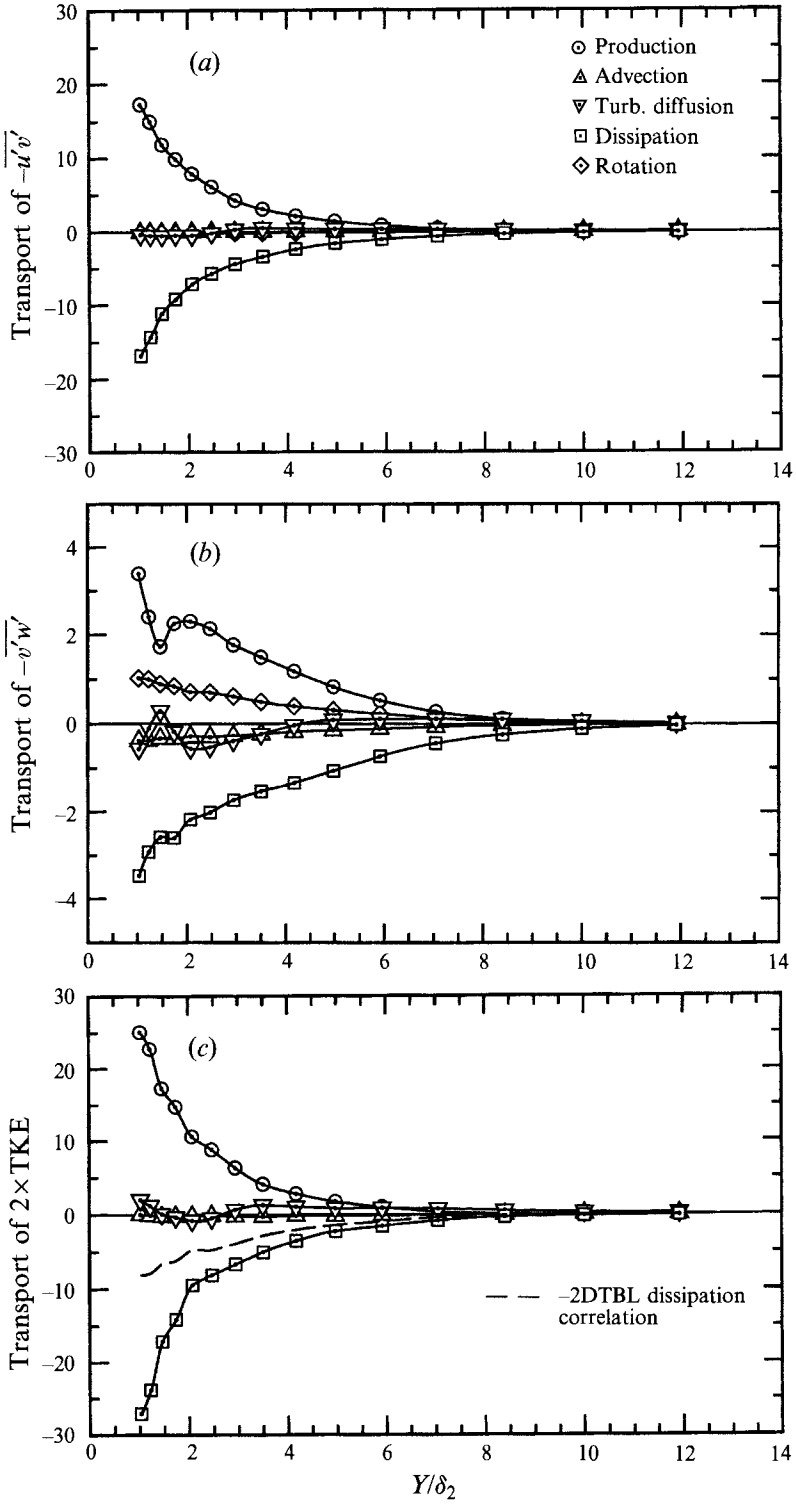

FIGURE 14. Transport equation balance for (*a*) $-\overline{u'v'}$, (*b*) $-\overline{v'w'}$ and (*c*) turbulent kinetic energy at $Re = 1300000$ normalized by δ/u_τ^3.

in the outer region which peaks at $Y/\delta \approx 0.5$. An almost imperceptible rise was seen in the disk flow dataset near the halfway point in the boundary layer, but is so small as to be almost lost on the axis. This discrepancy is at least partly due to the unmeasurable pressure fluctuation components in the turbulent diffusion, which are relatively more important in the outer region and are included in the numerical results.

Specifically relevant to this flow are the Coriolis redistribution terms and their effect on the evolution of the Reynolds stresses. As seen in the transport equations above, the rotation tends to provide a path by which the two important shear stresses can trade places. The value of $-\overline{u'v'}$ was shown earlier to be generally much larger than $-\overline{v'w'}$. This means that the 'trading' afforded by the Coriolis terms is unbalanced, with $-\overline{u'v'}$ losing much more than it gains from $-\overline{v'w'}$. These motions are of course not 'lost' or 'gained', but are merely redirected by the Coriolis effect, which is only a deflecting force and does no work. The direct rotation terms are thus seen to be small in comparison with the production and dissipation, suggesting that the timescale of rotation is much longer than that of the production and dissipative motions. A similar conclusion was reached by Spalart (1989). It would be a mistake to dismiss the rotation as irrelevant, because it also affects the development of each term in the stress transport equation, thus its effects are indirect. The direct rotation effect is small in the region we could measure, and it is likely that as the wall is approached the turbulent timescales get even smaller, suggesting the production and dissipation will continue to dominate the transport equation for $-\overline{u'v'}$.

The transport balance of the secondary, or cross-stream shear stress is shown in figure 14(*b*). This is plotted on an expanded scale relative to the $-\overline{u'v'}$ balance. Here the Coriolis term is shown to be much more significant. If the measurements were to extend closer to the wall where $\partial W/\partial y$ passes through zero and $-\overline{v'w'}$ changes sign, a dramatic change would be seen. The production term must pass through zero while the rotation term does not. Therefore, at the peak in the crossflow profile, the only positive term in the $-\overline{v'w'}$ balance comes from the Coriolis redistribution of $-\overline{u'v'}$. Instead of the rotation and the production augmenting each other to increase the magnitude of $-\overline{v'w'}$, the rotation will resist the formation of the shear stress needed to smear out the cross-stream velocity gradient. Thus the rotation would tend to allow a steep velocity profile near the wall by cutting down on the turbulent transfer of momentum. The dip seen in the production of $Y/\delta_2 \approx 1.5$ and a simultaneous decrease in turbulent diffusion seem to be real trends since they involve several points. These particular terms have uncertainties in the same order as the Reynolds stresses and are results of both mean and fluctuating measurements which were obtained with two different probes.

The remaining transport equation to be considered describes the development of twice the turbulent kinetic energy, shown in figure 14(*c*). Also shown on this plot is an empirical formula for the dissipation which is of the form

$$\epsilon = \frac{(\overline{u'v'}^2 + \overline{v'w'}^2)^{\frac{3}{2}}}{0.1\delta}, \tag{4}$$

which Bradshaw & Pontikos (1985) showed to do well in the two-dimensional section of their experiment, but to underpredict the dissipation in the three-dimensional section. It likewise badly underpredicts the dissipation in the disk flow, probably because of structural changes over the entire boundary layer compared with the two-dimensional case. Comparison of the measured quantities with 2DTBL's and the 3DTBL of Bradshaw & Pontikos (1985) show the disk production to drop off much closer to the wall than the others. The same quick drop was seen in the 3DTBL simulation of Spalart (1989).

From these measurements it seems clear that the disk boundary layer is dominated by the near-wall region, and that in the outer region inactive motions are perhaps even more prevalent than in 2DTBL's. This was highlighted by the monotonic drop in A_1 and the trend seen for the ratio $(\overline{u'^2}+\overline{w'^2})/\overline{v'^2}$, which clearly rises through the boundary layer while both 2DTBL's and other 3DTBL's fall monotonically away from the wall. These suggest that while there is no lack of turbulent motion, the mean transport of momentum by the Reynolds shear stresses is somehow curtailed.

It remains to address the cause of the reduced level of shear stress in the disk boundary layer. Bradshaw & Pontikos (1985) hypothesized that turbulent eddies formed in a two-dimensional boundary layer are tilted out of their preferred orientation by the imposition of three-dimensional skewing. Implicit in their discussion was the assumption that normal boundary-layer turbulence would eventually develop if the three-dimensional strain field remained constant for a long enough distance. Anderson & Eaton (1989) theorized that the turbulence is stabilized in the region of peak turbulence production by the presence of crossflow. Eaton (1991) took this further, stating that production is reduced because a fraction of the low-speed streaks in the boundary layer are eliminated by the crossflow and because longitudinal vortices are attenuated by the crossflow. Implicit in this argument is the assumption that boundary-layer turbulence developed in a three-dimensional strain field is inherently less efficient at extracting energy from the flow field. The present results support the latter hypothesis. The value of A_1 is suppressed below normal two-dimensional levels even though the entire boundary-layer development occurs in a nearly constant three-dimensional strain field.

5. Two-point correlations

Two-point velocity measurements were acquired to gain insight into the structural causes of reduced shear stresses in 3DTBL's. It is generally agreed that hairpin (or half-hairpin) vortices are important if not dominant features of 2DTBL's contributing much of the shear stress especially close to the wall. Our working hypothesis is that the structure is similar in the disk boundary layer with distortions accounting for the observed changes in the Reynolds stresses. Therefore, we have interpreted the two-point measurements in terms of the qualitative model presented by Robinson (1991). In a two-dimensional boundary layer, half-hairpins with either sign must be equally likely and two-point correlations with cross-stream separations must be symmetric or strictly antisymmetric. As will be seen below, asymmetries in the two-point correlations for the disk boundary layer give clues to the underlying structural modification. Quite extensive two-point measurements were acquired and are available in Littell & Eaton (1991*b*). Those presented here are selected as the most useful in illustrating structural disturbances.

Two-point velocity correlations have been documented by Grant (1958) and Tritton (1967) for the two-dimensional turbulent boundary layer, but none are available for a three-dimensional boundary layer. The two-point velocity correlation coefficient is most commonly defined as

$$R_{ij}(r_1, r_2, r_3) = \frac{\overline{u_i' u_j'}}{(\overline{u_i'^2})^{\frac{1}{2}}(\overline{u_j'^2})^{\frac{1}{2}}}, \tag{5}$$

where the subscript i refer to a velocity fluctuation at some point in space and the subscript j refers to a velocity fluctuation at some other location displaced from the first point by the vector (r_1, r_2, r_3).

Recently, the full simulations of boundary-layer and channel flow have yielded complete maps of the velocity correlations, and an examination of a subset of these data provided by O. Sendstad (1991, personal communication) supports the findings of the physical experiments. Notably, the structures seem to be about four times longer than they are wide in the spanwise direction for wall-normal and streamwise velocity correlations.

Two crosswires mounted on a common stem with variable separation were used to acquire all the two-point velocity data to be presented here. The probe was constructed with a 4° angle between the axis of each crosswire and the midline to allow a smaller separation between the measurement volumes of the crosswires than if they were parallel. The midline was aligned with the mean flow direction so the separation was normal to the laboratory streamline direction, but was not normal to the streamlines in the rotating reference frame. Since the correlations to be studied are seen in two dimensions to be much longer in the streamwise than the spanwise direction and because we effectively have a 'flying' hot wire, it was decided to make do with the few degrees of non-perpendicularity in the rotating coordinate system. This course of action also circumvents possible sources of error due to having one crosswire slightly ahead of the other in the laboratory frame. The measurements to be reported were all acquired at a height of 1.641 mm with separations ranging from 1.0 to 15.0 mm. The 'outboard' side of the stationary probe is in the positive radial direction and conversely the negative side of the stationary probe will be called 'inboard'. Data were taken at $Re = 650000$ and $Re = 1300000$ to check for Reynolds-number effects.

A check of the data accuracy is to examine the effect of separation on quantities measured by each probe individually. The values measured by each probe for the one-point correlation R_{uv} as a function of separation compared very well with that measured by a single probe, implying that systematic errors due to interference were insignificant. Higher-order statistics also agreed well, further supporting this conclusion.

Measurements of R_{11} and R_{22} are omitted here for brevity. Generally the results agree with the previous measurements of Grant (1958) and Tritton (1967). The present measurements of R_{11} were almost identical to those given by Tritton (1967) but the scales of motion implied by R_{22} have a somewhat larger spanwise extent than Tritton's, probably due to the different heights used. The R_{22} measurements of Tritton disagree with those of Grant (1958), whose $R_{22}(0, 0, r)$ does not show a negative region at any height. The present R_{22} measurements show a negative region, but obviously cannot be used to substantiate Tritton because of the three-dimensionality.

Figure 15 shows R_{12} at a height of 1.641 mm for two Reynolds numbers. Here a positive separation is in the direction of the crossflow (radially outward), and the solid symbols on the ordinate are from the Reynolds stress measurements made with a single crosswise in an earlier test. Redundant measurements using different probe orientations are also shown. Immediately apparent are the large symmetry and the difference in scale on each side of the stationary probe. This asymmetry is impossible in a two-dimensional boundary layer, but is quite clear for this three-dimensional flow. Comparison with Tritton (1967) implies that the strong dip on the negative axis is present in the two-dimensional boundary layer, and the lack of a dip on the positive axis is the effect of three-dimensionality. The R_{13} and R_{23} correlations generally support the existence of asymmetry, but are not definitive; see Littell & Eaton (1991*b*). Asymmetry provides direct evidence of structural modification by the three-dimensionality. The cause of this asymmetry is discussed below. Correlations involving the w' component of velocity, namely R_{13} and R_{23}, were also measured, both of which

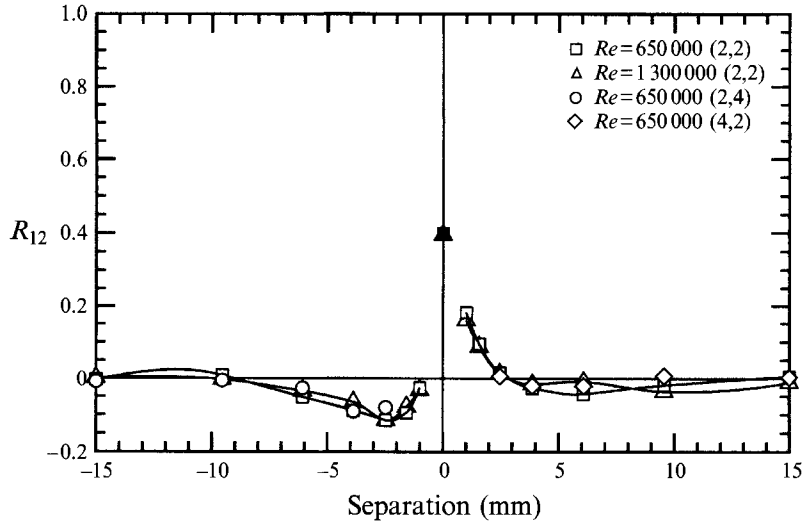

FIGURE 15. $R_{12}(0,0,r)$ for $Y = 1.641$ mm which equals $\overline{u'v'}$ at zero separation and shows strong asymmetry due to three-dimensionality.

are required to be antisymmetric in a 2DTBL. These quantities both showed asymmetry, but the cause was unclear.

6. Conditionally averaged velocity fields

Since we are most interested in structural changes that affect the development of Reynolds shear stresses, it appears most advantageous to study the two-point velocity correlations conditioned on a high level of shear stress. That is, we are looking at the average velocity field in the neighbourhood of a high-shear-stress event. In the discussion to follow we must be very clear of our nomenclature. An ejection is defined in the usual way as wall fluid moving outward, and a sweep as outer-layer fluid moving down. Examining the disk flow in laboratory coordinates, the wall fluid has a high value of u. Therefore plotting a velocity measurement in the usual way with u' on the abscissa and v' on the ordinate, an ejection is a quadrant-1 event and a sweep is a quadrant-3 event.

Figure 16 shows the distribution of contributions to the value of $\overline{u'v'}$ in the form of a joint probability density function weighted by the value of each event's product $u'v'$. These data were computed using a subset of the results of the two-point measurements for $Re = 650000$ at a height of 1.641 mm. It can be clearly seen that the ejection and the sweep events contribute much more heavily to the mean than the other two quadrants. Events falling in the areas defined by the curves $u'v' \geqslant 2u'_{rms}v'_{rms}$, will be considered relatively strong sweeps or ejections, as discriminated from events which do not contribute strongly to the Reynolds stress $\overline{u'v'}$. Using this criterion, about 4.5% of the total number of events were identified as energetic ejections and about 2.4% of the total were strong sweeps.

In addition to conditional sampling based on either a strong sweep or a strong ejection, the state of the flow field when a simple vertical motion of either sign was detected was also investigated. The condition used for this was that $|v'|$ exceed $\sqrt{2}v'_{rms}$. These will be referred to as 'rising' or 'sinking' flow, and by figure 16 it can be seen that the ejection and sweep conditions can be thought of as restricted versions of the rising and sinking conditions respectively.

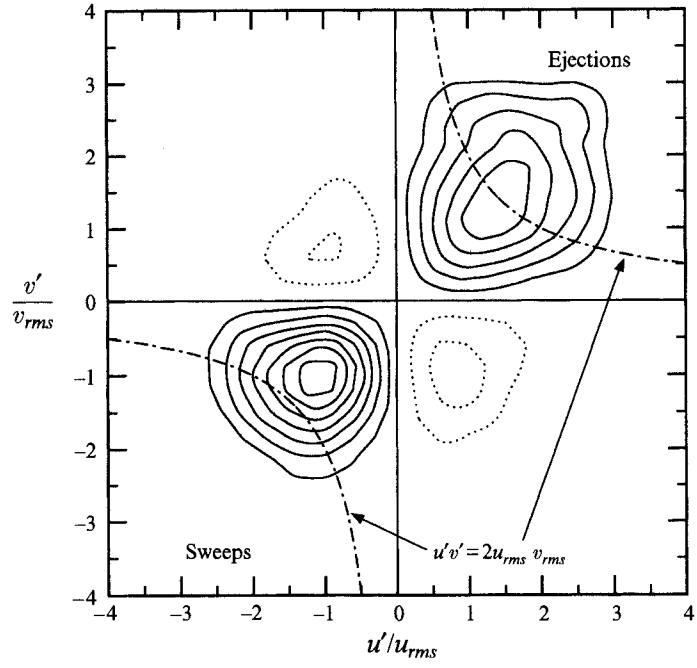

FIGURE 16. Joint probability density function weighted by the product $u'v'$ showing likelihood of contribution to $\overline{u'v'}$; positive contributions are solid contours, negative contributions are dashed.

The main subject of interest is the structure that produces Reynolds shear stress in the log region, which for a two-dimensional wall-bounded shear flow is likely to resemble the half-hairpin shown by Robinson (1991). The feature of this structure most easily identified by two-point velocity measurements separated in the spanwise direction is the closely spaced upward and downward motion on either side of the trailing neck vortex. A measure of how effective the structure may be at rearranging boundary-layer fluid could be deduced from the streamwise velocity distribution. As the various plots are introduced in the following sections, a few simpler structural models which preceded Robinson (1991) will be discussed to test their applicability in this flow.

6.1. *Upward motion*

Figure 17(*a*) shows the average vertical motion surrounding a rising event, normalized by the r.m.s. of the unconditioned wall-normal velocity fluctuations. Each of the plots of this type are scaled using the pertinent r.m.s. quantity, with the values at zero separation given in the caption for reference. Just as the correlation coefficients were seen to asymptote to zero at large separations, these averages will approach zero as the separation increases. This plot shows a striking symmetry which suggests the equal probability of sinking flow at some small separation (3 mm) in the $Re = 650000$ case. This implies the presence of an equal number of positively and negatively signed longitudinal vortices producing an upward flow detected as the rising event, and downward flow on the other side of their cores. The pattern found in the $Re = 1300000$ case is also symmetric, but does not have the strong dips seen for the lower Reynolds number, an indication of some kind of scaling with Reynolds number for this quantity. Since the total boundary-layer thickness is almost constant while the viscous lengthscale has been halved by raising the Reynolds number from 650000 to 1300000,

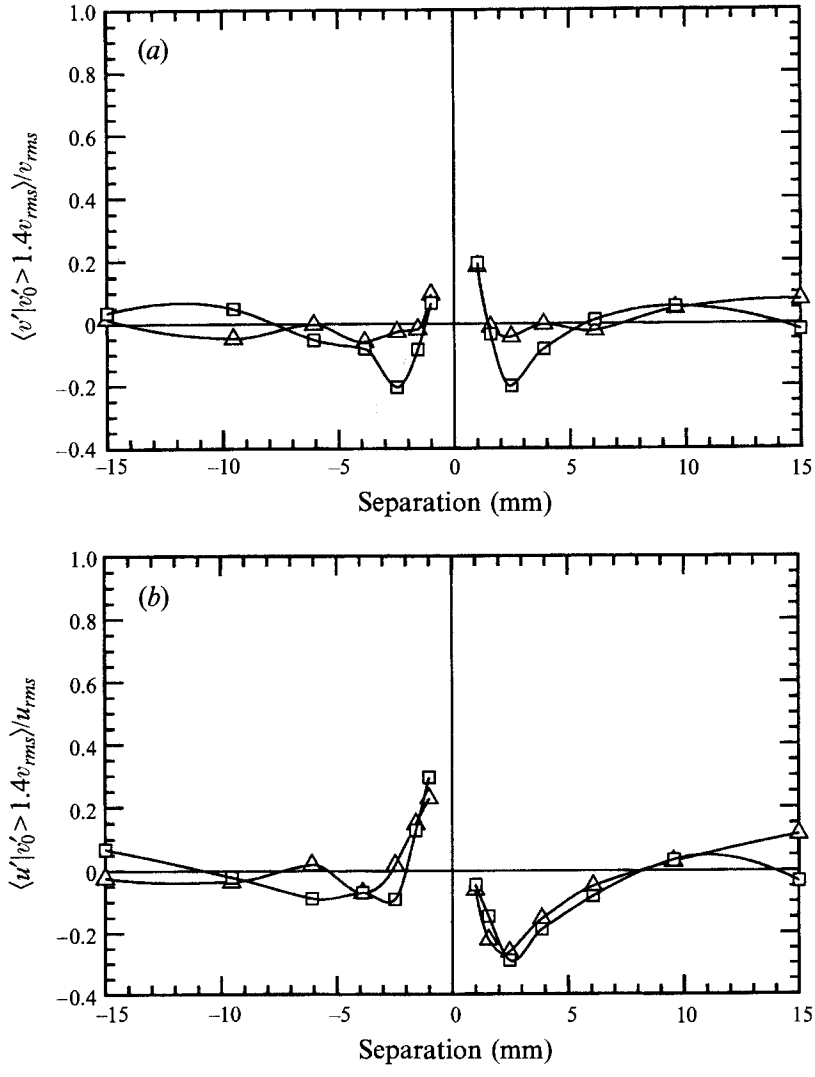

FIGURE 17. (*a*) Average vertical motion around a rising event, showing symmetry or an equal likelihood of each sign of streamwise vortex. (*b*) Average streamwise fluctuations around a rising event, showing asymmetry due to unequal effect of each sign of streamwise vortex. □, $Re = 650000$; △, $Re = 1300000$. Zero separation: (*a*) □ = 2.00, △ = 1.61; (*b*) □ = 0.82, △ = 0.78. $Y = 1.641$ mm.

(see table 2), a wall dependence of the structures causing a rising event might be inferred.

Figure 17(*b*) shows how the streamwise velocity is modified on average when a rising event is detected. This implies that the vortices shown in figure 17(*a*) do not warp the *u*-contours of the boundary-layer fluid evenly. Even though both signs of longitudinal vortex exist and can produce vertical motion, they, or more precisely whatever structure they are part of, affect the boundary layer in an asymmetric fashion. No Reynolds-number effect is observed for this quantity, which undermines the existence of wall scaling for the rising event.

When the condition is changed to a strong ejection event, the vertical and streamwise velocity averages take the form shown in figures 18(*a*) and 18(*b*) respectively.

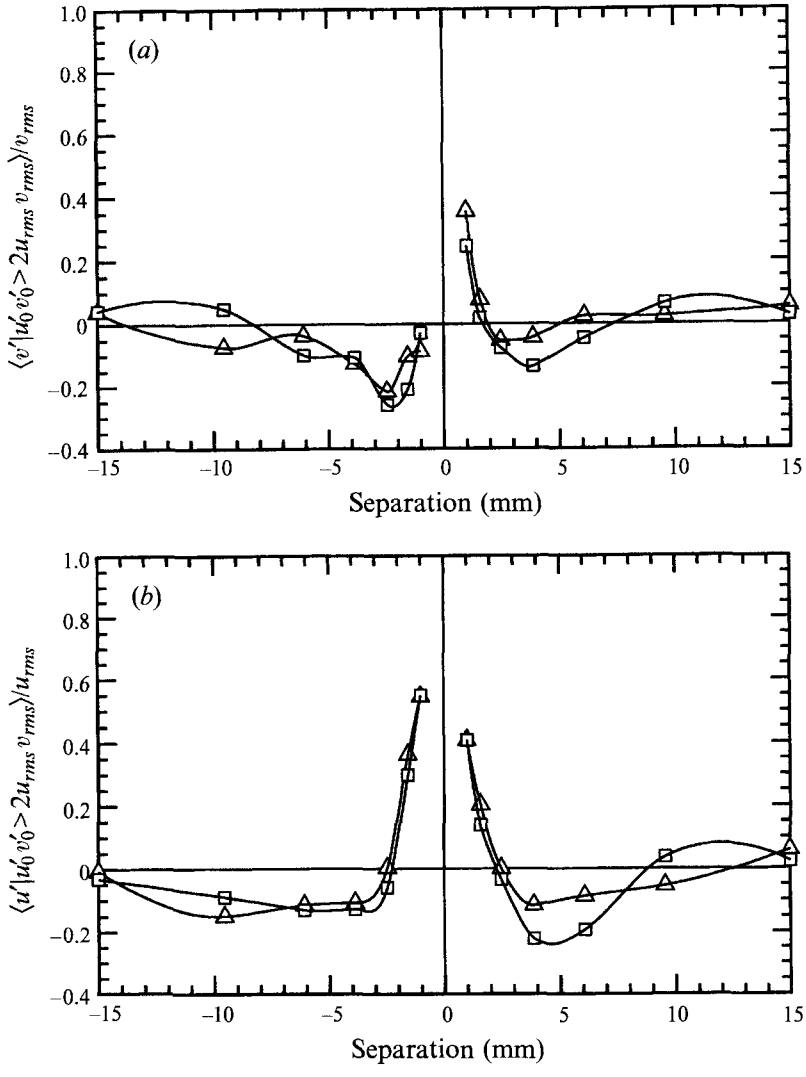

FIGURE 18. (*a*) Average vertical motion around an ejection event, showing asymmetry due to unequal effect of each sign of streamwise vortex. (*b*) Average streamwise fluctuations around an ejection event. □, $Re = 650000$; △, $Re = 1300000$. Zero separation: (*a*) □ = 1.97, △ = 1.90; (*b*) □ = 1.79, △ = 1.77. $Y = 1.641$ mm.

Interestingly, the situation described for the rising condition is nearly reversed with the asymmetry being exhibited by the vertical fluctuations and a much more nearly symmetric streamwise velocity distribution. Figures 17(*b*) and 18(*a*) dismiss the existence of any symmetric structure, or equal effects on the boundary layer of mirror images of some asymmetric structure including models based on full horseshoe or complete hairpin structures, Townsend's (1976) double cone rollers, and in general any symmetric pairs of streamwise vortices. The picture emerging is that an even population of each sign of longitudinal vortex exists, but that one sign is associated with a structure that is better at producing ejections.

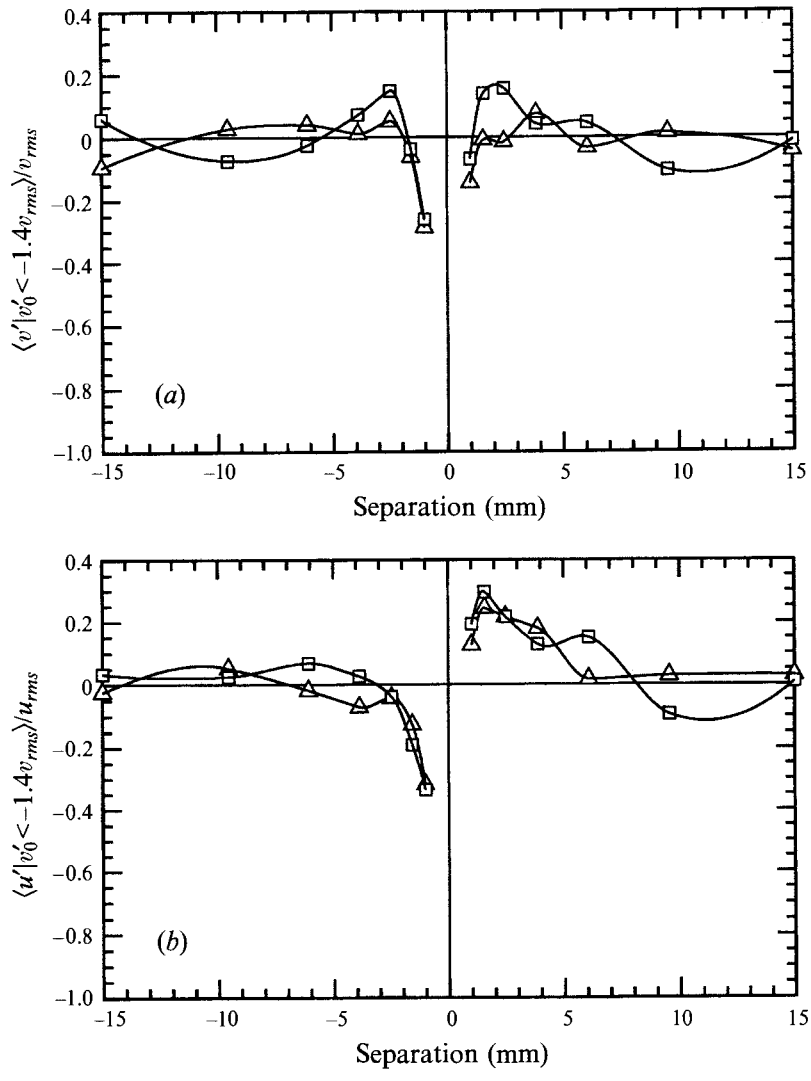

FIGURE 19. (*a*) Average vertical motion around a sinking event, suggesting symmetry or an equal likelihood of each sign of streamwise vortex. (*b*) Average streamwise fluctuations around a sinking event, showing asymmetry due to unequal effect of each sign of streamwise vortex. □, $Re = 650000$; △, $Re = 1300000$. Zero separation: (*a*) □ $= -1.80$, △ $= -1.83$; (*b*) □ $= -0.48$, △ $= -0.55$, $Y =$ 1.641 mm.

6.2. *Downward motion*

Figure 19(*a*) shows the average vertical motion surrounding a sinking event, showing roughly the same behaviour as seen for the rising event, i.e. general symmetry suggesting equal probability of each sign of vortex. Also seen is the same sort of Reynolds-number effect which attenuates the overshoot at small separation from the condition event.

Figure 19(*b*) shows the conditionally averaged streamwise velocity fluctuations during sinking events. This implies that the vortices shown in figure 19(*a*) do not warp the *u*-contours of the boundary-layer fluid evenly, and an overshoot is noted on the outboard side of the event, while inboard contours just asymptote to the average of

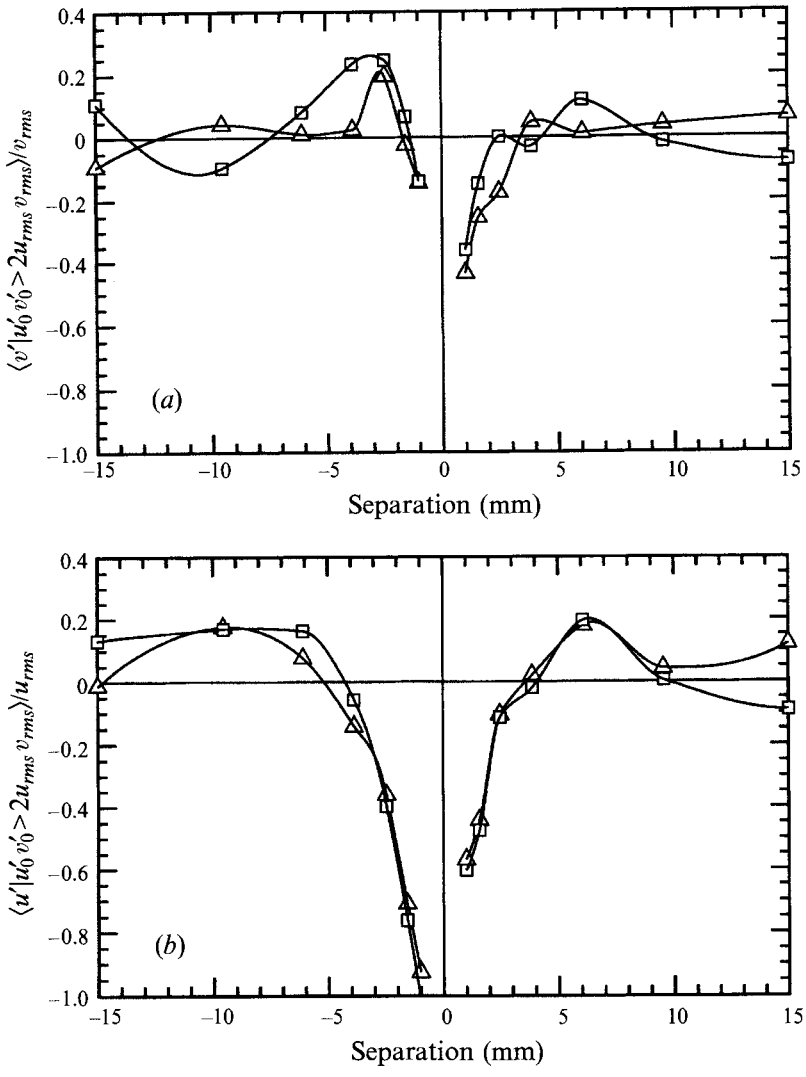

FIGURE 20. (*a*) Average vertical motion around a sweep event, showing asymmetry due to unequal effect of each sign of streamwise vortex. (*b*) Average streamwise fluctuations around a sweep event. □, $Re = 650000$; △, $Re = 1300000$. Zero separation: (*a*) □ $= -1.63$, △ $= -1.67$; (*b*) □ $= -1.68$, △ $= -1.71$. $Y = 1.641$ mm.

$u' = 0$. This is exactly the effect seen for the rising case in figure 17(*b*), and again no Reynolds-number effect is observed for this quantity, just as noted for the rising event.

Figures 20(*a*) and 20(*b*) are conditioned on the sweep event. Figure 20(*a*) shows that restricting the condition from simple sinking flow to a strong sweep event accentuates the presence of an inboard vortex, while the outboard vortex is not detected. The extent of the distortion of the streamwise velocity contours is shown in figure 20(*b*), which shows a certain asymmetry in its approach to zero, but lacks the clear asymmetry in the overshoot region seen in figure 19(*b*). The asymmetry of the v'-averaged motion suggests that one sign of vortex is more efficient at producing a sweep than the other sign, as was concluded for the ejection event above.

7. Discussion

Unfortunately it is usually easier to disprove hypothetical structures than to unequivocally demonstrate support for a particular structure model. It was stated during the discussion of the ejection condition that all symmetric models, including those with even distributions of mirror-imaged asymmetric structures, could not produce the two-point velocity correlation presented here. These measurements will therefore be interpreted as a description of how the structure described by Robinson (1991) might be modified by the presence of spanwise shear. That structure is an arch-like vortex which trails behind it a neck inclined at some angle to the wall and a tail which extends in a generally streamwise direction parallel to the wall. The sense of rotation of the arch is the same as the mean spanwise vorticity of the boundary layer, and the neck and tail emanate with equal likelihood from either side of an arch, but each arch is generally found to have a tail on one side only. This important feature differentiates this model from those based on symmetric horseshoe vortices. Robinson (1991) presented this as the consensus view of a shear-stress-producing structure in the log region of a 2DTBL from the record of many physical experiments and direct numerical simulations. The same general type of structure could be expected in a perturbed 2DTBL, such as a turning flow producing a 3DTBL, though it may be modified by the extra mean shear. In the rotating reference frame the similarity between the disk flow and other 3DTBL's has been shown by the mean flow and single-point statistics to be substantial, and it may thus be inferred that the same type of structures would exist in each of these wall-bounded shear flows.

Following the nomenclature of Shizawa & Eaton (1991) for relating vortex sign to the mean crossflow velocity profile, a Case 1 streamwise vortex is that with a secondary velocity which augments the crossflow close to the surface, while the Case 2 secondary velocity is opposite to the crossflow near the wall. Here we will designate the two possible arch orientations as Case 1 and Case 2 structures by virtue of the relationship of their streamwise tails with the crossflow.

Robinson (1991) stated that strong ejections were most commonly found upstream of an arch inside a neck, and strong sweeps were found on the outside of the neck. Since an arch with a single neck is more common than one with two, the relative spanwise location of sweeps and ejections seems to be a likely way to differentiate Case 1 from Case 2 in instantaneous two-point velocity correlations. The streamwise location of the sweep and ejection are of course not required to be exactly the same, which considerably increases the amount of data needed to completely define the structure being measured. It will therefore by assumed that on average they occur side-by-side for the purposes of this discussion. This is not a major concern for the unconditioned two-point correlations, but may have an impact on the applicability of the conditioned measurements in a manner which is difficult to predict.

We are now ready to advance a description of coherent structure modification by spanwise shear, based on Robinson's 2DTBL structure. Like all structural models, sufficient information for proof is not available, but the model presented here does fit all the peculiar trends noted above. It also has the advantage of being very simple to describe, though the dynamic mechanism causing the modification is somewhat harder to envision.

From a combination of evidence of rising and ejection events, we conclude that most strong ejections are caused by Case 1 structures as shown in figure 21. Figure 15, R_{12}, shows quite clearly that asymmetries exist in this 3DTBL which are impossible in a 2DTBL. Two-point correlations conditioned on the presence of Reynolds shear stress

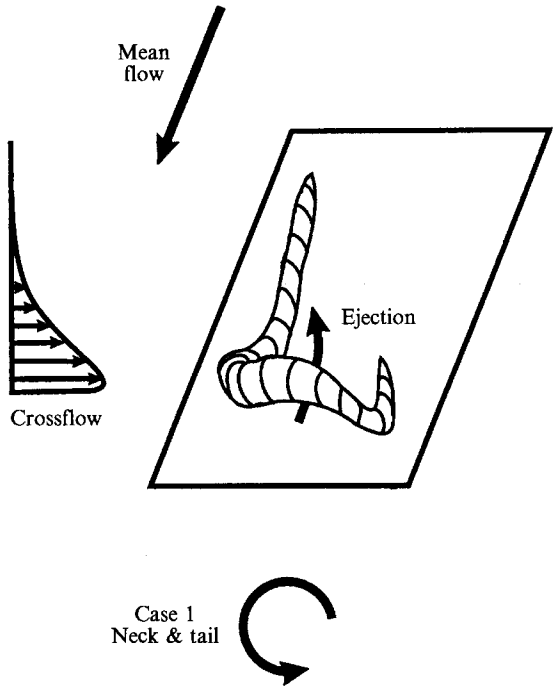

FIGURE 21. Shear stress structure of Robinson (1991) with Case 1 neck and tail as modified by three-dimensionality.

were evaluated to see if they caused the asymmetry, and correlations conditioned on the presence of simple vertical motion were used to test for streamwise vorticity. Figure 17(*a*), $\langle v' | \text{rising} \rangle$, shows that both Case 1 and Case 2 vortices can cause upward vertical motion, but figure 18(*a*), $\langle v' | \text{ejection} \rangle$, shows that Case 1 structures are responsible for most ejections. Taken together, these support the scenario depicted in figure 21, showing that structures with Case 1 necks and tails are responsible for most strong ejections.

Conversely, figure 22 shows the proposed mechanism for production of strong sweeps by Case 2 structures, as deduced from the sinking and sweep conditionally averaged events. Figure 19(*a*), $\langle v' | \text{sinking} \rangle$, shows that both Case 1 and Case 2 vortices can cause vertical motion downward, but figure 20(*a*), $\langle v' | \text{sweep} \rangle$, shows that Case 2 structures are producing more of the strong sweeps, owing to the lack of upward motion outboard of the sweep as would be expected from a Case-1-triggered event.

The ejection and sweep criteria taken together indicate that the neck of a Case 1 structure loses its ability to produce a sweep. The relatively weak downward motion outboard of the ejection means that the arch of a Case 2 structure is somehow being modified and is not producing strong ejections, but is causing sweeps.

The dynamics of the structural interaction with the crossflow velocity is open to interpretation, and could be very different for each unique structure and only average out to give the asymmetric behaviour noted here. One possible interpretation involves the Case 1 neck and tail (figure 21) simply rolling up the inflexional crossflow velocity profile instead of pumping fluid down and producing a strong inboard sweep. This rolling up of vorticity would be less likely to disturb, and would probably strengthen, the ejection upstream of the arch. If a Case 2 structure interacts with the crossflow, it could ruin the ejection upstream of the arch by opposing the secondary flow of the neck

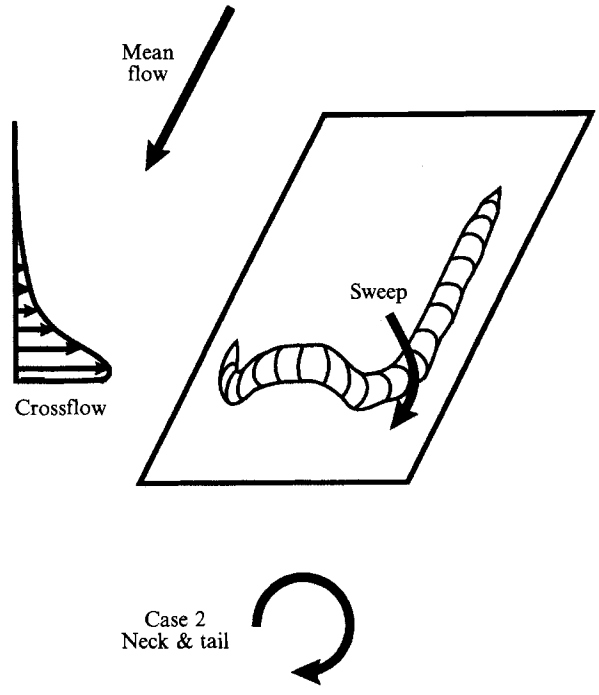

FIGURE 22. Shear stress structure of Robinson (1991) with Case 2 neck and tail as modified by three-dimensionality.

on the inboard side, while having a smaller effect on the outboard sweep as shown in figure 22. Both of these structure modifications can be summarized as requiring some part of the structure to be inboard of the surviving event (sweep or ejection); thus the inboard feature 'protects' the outboard event from the crossflow velocity profile.

8. Summary

Several sets of mean and turbulent fluctuation measurements were obtained at multiple radii and speeds to document the turbulent flow field up to $Re_{\delta_2} = 6000$. The present data agreed well with previous mean measurements, and agreed qualitatively with the few turbulence measurements available for 'infinite' disk flow. It was demonstrated that the peak in the crossflow profile does not scale on inner variables, but outer-variable scaling could not be established owing to the uncertainty in measuring the total boundary-layer thickness.

It was concluded that the disk boundary layer is dominated by the near-wall region, and that in the outer region inactive motions are even more prevalent than in two-dimensional boundary layers. The ratio of the shear stress vector magnitude to the turbulent kinetic energy, A_1, was at a maximum near the wall at close to the two-dimensional value, but dropped off almost linearly away from the wall. The reduction in A_1 in the outer region of the disk-flow boundary layer suggests that the modification of A_1 observed in 3DTBL's is not merely a disequilibrium effect. More research is needed to determine the generality of this conclusion. The primary shear stress $-\overline{u'v'}$ normalized by the wall friction velocity was seen to have a value of 0.6 at $y^+ = 110$, which is considerably lower than in a 2DTBL at the same Reynolds number. This indicates a very small, or non-existent, constant Reynolds shear stress region near the

wall. The shear stress vector and the mean flow strain-rate vector were found to be closely aligned throughout the boundary layer, as opposed to 3DTBL's produced by strong skewing of a 2DTBL.

The Reynolds stress transport equation balances showed that the direct effects of rotation (Coriolis effects on the turbulence), are negligible for the primary shear stress $-\overline{u'v'}$, but make a large contribution to the development of the secondary shear stress $-\overline{v'w'}$. Traditional 2DTBL estimates of turbulent lengthscales based on shear stress were seen to perform poorly, while those based on turbulent kinetic energy worked well. A new model proposed by Hunt *et al.* (1987) failed badly in its original form based on v'-fluctuations. This was concluded to be a result of the low values of $\overline{v'^2}$ found for the disk flow.

Two-point velocity correlations showed quite clearly that strong asymmetries exist in this three-dimensional boundary layer so symmetric structure models are inappropriate. The structural model of Robinson (1991) consisting of vortical arches each with a single quasi-streamwise vortical leg was found to be plausible if interaction with the crossflow is taken into account. Conditionally sampled two-point correlations showed that structures with a leg on the inboard side of the arch produced strong ejections but weakened sweeps. Oppositely signed structures produced strong sweeps but weakened ejections.

The turbulent stress data presented here are limited to the logarithmic and outer regions of the boundary layer, as in most other three-dimensional boundary-layer experiments. Extension of the Reynolds stress measurements to the near-wall region would shed considerable light on the processes at work nearer the peak in the production of turbulent kinetic energy.

Two-point velocity correlations from other three-dimensional boundary layers, particularly those based on 'infinite' geometries, are needed to evaluate coherent structure models as modified by three-dimensionality. Direct numerical simulations will probably continue to be the best source of coherent structural information, but extension to high Reynolds numbers will require more laboratory experiments into the effects of three-dimensionality.

This work is supported by the Department of Energy Office of Basic Energy Science Grant DE-FG03-86ER13608. The first author would also like to express his appreciation for the support in the form of a scholarship from the Society of Experimental Test Pilots.

REFERENCES

ANDERSON, S. D. & EATON, J. K. 1987 An experimental investigation of pressure driven three-dimensional boundary layers. *Stanford Univ., Dept. Mech. Engng Thermosciences Div. Rep.* MD-49.

ANDERSON, S. D. & EATON, J. K. 1989 An experimental investigation of pressure-driven three-dimensional boundary layers. *J. Fluid Mech.* **202**, 263–294.

BERG, B. VAN DEN, ELSENAAR, A., LINDHOUT, J. P. F. & WESSELING, P. 1975 Measurements in an incompressible three-dimensional turbulent boundary layer, under infinite swept wing conditions, and comparison with theory. *J. Fluid Mech.* **70**, 127–148.

BISSONNETTE, L. R. & MELLOR, G. L. 1974 Experiments on the behaviour of an axisymmetric turbulent boundary layer with a sudden circumferential strain. *J. Fluid Mech.* **63**, 369–413.

BRADSHAW, P. 1970 Calculation of three-dimensional turbulent boundary layers. *J. Fluid Mech.* **46**, 417–445.

BRADSHAW, P., FERRIS, D. H. & ATWELL, N. P. 1967 Calculation of boundary-layer development using the turbulent energy equation. *J. Fluid Mech.* **28**, 593–616.

BRADSHAW, P. & PONTIKOS, N. S. 1985 Measurements in the turbulent boundary layer on an 'infinite' swept wing. *J. Fluid Mech.* **159**, 105–130.

BRADSHAW, P. & SENDSTAD, O. 1990 Structure of three-dimensional boundary layers. *Center for Turbulence Research Proc. Summer Progam, 1990.*

BRADSHAW, P. & TERRELL, M. C. 1969 The response of a turbulent boundary layer on an 'infinite' swept wing to the sudden removal of pressure gradient. *NPL Aero Rep.* 1305.

CASE, P. 1966 Measurements of entrainment by a free rotating disk. *J. R. Aero. Soc.* **71**, 124.

CEBECI, T. & ABBOTT, D. E. 1975 Boundary layers on a rotating disk. *AIAA J.* **13**, 829–832.

CHAM, T.-S. & HEAD, M. R. 1969 Turbulent boundary-layer flow on a rotating disk. *J. Fluid Mech.* **37**, 129–147.

CIMBALA, J. M. & PARK, W. J. 1990 a direct hot-wire calibration technique to account for ambient temperature drift in incompressible flow. *Exp. Fluids* **8**, 299–300.

COBB, E. C. & SAUNDERS, O. A. 1956 Heat transfer from a rotating disk. *Proc. R. Soc. Lond.* A **236**, 343–351.

COLEMAN, G. N., FERZIGER, J. H. & SPALART, P. R. 1990 A numerical study of the turbulent Ekman layer. *J. Fluid Mech.* **213**, 313–348.

CUTLER, A. D. & JOHNSTON, J. P. 1989 The relaxation of a turbulent boundary layer in an adverse pressure gradient. *J. Fluid Mech.* **200**, 367–387.

DECHOW, R. & FELSCH, K. O. 1977 Measurements of the mean velocity and of the Reynolds stress tensor in a three-dimensional turbulent boundary layer induced by a cylinder standing on a flat wall. *Proc. 1st Turbulent Shear Flow Symp., University Park, Pennsylvania, Apr. 18–20.*

DRIVER, D. M. & JOHNSTON, J. P. 1990 Experimental study of a three-dimensional shear-driven turbulent boundary layer with streamwise adverse pressure gradient. *NASA TM* 102211; and *Stanford Univ., Dept. Mech. Eng. Thermosciences Div. Rep.* MD-57.

EATON, J. K. 1991 Turbulence structure and heat transfer in three-dimensional boundary layers. *Proc. 9th Symp. on Energy Engineering Sciences, Argonne Natl Lab.*

ELSENAAR, A. & BOELSMA, S. H. 1974 Measurements of the Reynolds stress tensor in a three-dimensional turbulent boundary layer under infinite swept wing conditions. *NLR TR* 74095 U.

ERIAN, F. F. & TONG, V. H. 1971 Turbulent flow due to a rotating disk. *Phys. Fluids* **14**, 2588–2591.

FERNHOLZ, H. H. & VAGT, J.-D. 1981 Turbulence measurements in an adverse-pressure-gradient three-dimensional turbulent boundary layer among a circular cylinder. *J. Fluid Mech.* **111**, 233–269.

GOLDSTEIN, S. 1935 On the resistance to the rotation of a disk immersed in a fluid. *Proc. Camb. Phil. Soc.* **31**, 232.

GRANT, H. L. 1958 The large eddies of turbulent motion. *J. Fluid Mech.* **4**, 149–190.

GREGORY, N., STUART, J. T. & WALKER, W. S. 1955 On the stability of three-dimensional boundary layers with application to the flow due to a rotating disk. *Phil. Trans. R. Soc. Lond.* A **248**, 155–199.

HUNT, J. C. R., SPALART, P. R. & MANSOUR, N. N. 1987 A general form for the dissipation length scale in turbulent shear flows. *Center for Turbulence Research, Proc. Summer Program*, 1987, pp. 179–184.

ITOH, M., YAMADA, Y., IMAO, S. & GONDA, M. 1990 Experiments on turbulent flow due to an enclosed rotating disk. *Intl Symp. on Turbulence Modelling and Measurements, Dubrovnik, Yugoslavia*, pp. 659–668.

JOHNSTON, J. P. 1970 Measurements in a three-dimensional turbulent boundary layer induced by a swept, forward-facing step. *J. Fluid Mech.* **42**, 823–844.

KÁRMÁN, T. VON 1921 Über Laminare und Turbulente Reibung. *Z. Angew. Math. Mech.* **1**, 233–252. (transl: On laminar and turbulent friction. *NACA Tech. Mem.* 1092 (1946)).

KLEBANOFF, P. S. 1954 Characteristics of turbulence in a boundary layer with zero pressure gradient. *NACA TN* 3178 (superseded by *NACA Rep.* 1247).

KOBAYASHI, R., KOHAMA, Y. & TAKAMADATE, CH. 1980 Spiral vortices in boundary layer transition regime on a rotating disk. *Acta Mechanica* **35**, 71–82.

KOHAMA, Y. 1987 Crossflow instability in rotating disk boundary-layer. *AIAA*-87-1340.

LIGRANI, P. M. & BRADSHAW, P. 1987 Spatial resolution and measurement of turbulence in the viscous sublayer using subminiature hot-wire probes. *Exp. Fluids* **5**, 407–417.

LITTELL, H. S. & EATON, J. K. 1991*a* The unsteady flowfield behind a vortex generator rapidly pitched to angle of attack. *AIAA J.* **29**, 577–584.

LITTELL, H. S. & EATON, J. K. 1991*b* An experimental investigation of the three-dimensional boundary layer on a rotating disk. *Stanford Univ., Dept. Mech. Engng Thermosciences Div. Rep.* MD-60.

LOHMANN, R. P. 1976 The response of a developed turbulent boundary layer to local transverse surface motion. *Trans. ASME* I: *J. Fluids Engng* **98**, 354–363.

MOIN, P., SHIH, T.-H., DRIVER, D. M. & MANSOUR, N. N. 1990 Direct numerical simulation of a three-dimensional turbulent boundary layer. *Phys. Fluids* A **2**, 1846–1853.

MULLER, U. & KRAUSE, B. 1979 Measurements of mean velocities and Reynolds stresses in an incompressible three-dimensional turbulent boundary layer. *Proc. 2nd Turbulent Shear Flows Symp.*, Imperial College, London, 1979, p. 15.36.

ROBINSON, S. K. 1991 Motions in the turbulent boundary layer. *Ann. Rev. Fluid Mech.* **23**, 601–639.

SENDSTAD, O. & MOIN, P. 1991 On the mechanics of 3-D turbulent boundary layers. *Proc. 8th Turbulent Shear Flow Symp.*, Munich, Germany, Sept. 9–11, pp. 5-4-1–5-4-5.

SENOO, Y. & NISHI, M. 1972 Equilibrium three-dimensional turbulent boundary layer on the end wall of a curved channel. *Proc. 2nd Intl JSME Symp., Tokyo, Japan, Sept. 1972*, pp. 21–30.

SHIZAWA, T. & EATON, J. K. 1992 Turbulence measurements for a longitudinal vortex interacting with a three-dimensional turbulent boundary layer. *AIAA J.* **30**, 49–55.

SPALART, P. R. 1988 Direct simulation of a turbulent boundary layer up to $Re_\theta = 1410$. *J. Fluid Mech.* **187**, 61–98.

SPALART, P. R. 1989 Theoretical and numerical study of a three-dimensional turbulent boundary layer. *J. Fluid Mech.* **205**, 319–340.

SQUIRE, H. B. & WINTER, K. G. 1951 The secondary flow in a cascade of airfoils in a nonuniform stream. *J. Aero. Sci.* **18**, 271–277.

THEODORSEN, T. & REGIER, A. 1944 Experiments on drag of revolving disks, cylinders and streamline rods at high speeds. *NACA Rep.* 793.

TOWNSEND, A. A. 1976 *The Structure of Turbulent Shear Flow.* Cambridge University Press.

TRITTON, D. J. 1967 Some new correlation measurements in a turbulent boundary layer. *J. Fluid Mech.* **28**, 439–462.

TUTU, N. K. & CHEVRAY, R. 1975 Cross-wire anemometry in high intensity turbulence. *J. Fluid Mech.* **71**, 785–800.

WESTPHAL, R. V. & MEHTA, R. D. 1985 Crossed hot-wire data acquisition and reduction system. *NASA TM* 85871.

WILKINSON, S. P. & MALIK, M. R. 1985 Stability experiments in the flow over a rotating disk. *AIAA J.* **23**, 588–595.